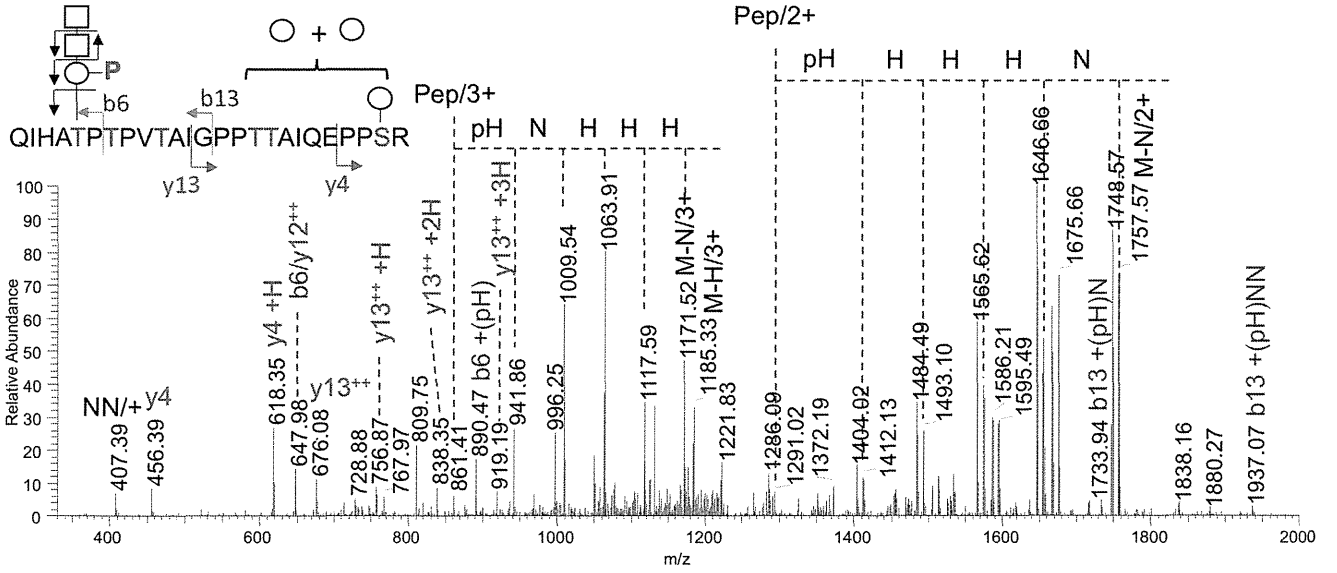

Figure 4 | Determination of the presence of a phosphorylated trisaccharide on T317 of α-DG428 co-expressed with AGO61 in COS7 cells. α-DG428 was purified using a HaloTag protein purification system from cell lysates co-transfected with α-DG428-HALO and AGO61, separated by SDS-PAGE, and in-gel digested with trypsin (Supplementary Fig. S6). The extracted peptides/glycopeptides were directly analyzed by LC-MS/MS. The successive neutral losses of HexNAc and PHex from both the doubly and triply charged molecular ions overlapped with those of the additional Hex and collectively defined the m/z of the bare peptide core with the fitted $P_1Hex_4HexNAc_2$ glycosyl composition. The y4 + Hex and y13 + Hex_{1-3} fragment ions localized the additional 3 Hex on the C-terminal half of the peptide, whereas the b13 + PHex + $HexNAc_{1-2}$ ions established the $HexNAc_2PHex$ substituent on the N-terminal half along with the b6 + PHex ion that further identified it on T317, as annotated. Key: Pep, peptide core; circle and H, Hex; square and N, HexNAc; P, phospho-; pH, phosphorylated Hex; M, molecular ion.

functional Xyl-GlcA repeats of laminin-binding glycans[12,27,28], whereas AGO61 was localized in the endoplasmic reticulum (ER) (Supplementary Fig. S2), consistent with the previously reported result obtained with HEK293 cells[21]. These results indicated that AGO61 was actively involved in an early stage of laminin-binding glycan formation.

AGO61 modifies GlcNAc residues at specific sites on α-DG. Most recently, it was reported that AGO61 had POMGnT activity, which contributed to the formation of a previously identified phosphorylated *O*-mannosyl trisaccharide [GalNAc-β3-GlcNAc-β4-(phosphate-6-)Man][21]. However, AGO61 belongs to the GT61 family, which includes the recently identified extracellular protein *O*-β-*N*-acetylglucosaminyltransferase. To detect all likely GlcNAc modifications by AGO61, we used an anti-*O*-GlcNAc antibody (clone: CTD110.6) with known wide cross-reactivity, including reactivity against terminal GlcNAc-β1-4GlcNAc[29] (Fig. 3a). AGO61-dependent GlcNAc modification was detected by CTD110.6 but not by another anti-*O*-GlcNAc antibody (HGAC85) (Supplementary Fig. S3). Interestingly, AGO61-dependent GlcNAc modifications were detected in α-DG-Fc prepared from cell lysates but not in those secreted into the medium irrespective of HFaq treatment (Fig. 3a and Supplementary Fig. S4).

To identify the AGO61-dependent GlcNAc modification sites on α-DG, we generated 3 types of α-DG deletion mutants with C-terminal HALO tags (Supplementary Fig. S5). AGO61-dependent GlcNAc modifications were detected in all these mutants, which indicated that the modification had occurred in the N-terminal 62-residue segment of the mucin-like domain. This domain contains the previously identified sites (Thr-317 and Thr-319) that display the laminin-binding glycans produced by LARGE[30]. Using α-DG373 and its T317A/T319A mutant, we confirmed that these threonine residues displayed laminin-binding glycans (Fig. 3b). Interestingly, the T317A/T319A mutant of α-DG373 exhibited little GlcNAc modification despite AGO61 expression (Fig. 3c).

Moreover, by LC-MS/MS analysis of the tryptic glycopeptides derived from recombinant α-DG428 expressed in the presence or absence of AGO61 in COS7 cells, among other glycoforms, we detected one that carried three Hex, two HexNAc, and a phosphorylated Hex (PHex) on QIHA^{317}TP^{319}TPVTAIGPPTTAIQEPPSR (Fig. 4). In accordance with the substrate specificity of SGK196, which phosphorylates the trisaccharide GalNAcβ-3GlcNAcβ-4Man but not the single Man[21], the detected b6 + PHex ion localized the phosphorylated trisaccharide at T317. This was corroborated by the b13 ions that carried an intact $HexNAc_2PHex$ moiety and Hex-containing y4 and y13 ions, which localized the additional *O*-Hex substituents at the C-terminal half distal from T317.

AGO61 is a priming enzyme for the formation of laminin-binding glycans. LARGE-dependent hyperglycosylation was undetectable for the T317A/T319A mutant of α-DG373, whereas the formation of laminin-binding glycans was slightly enhanced when LARGE was co-overexpressed with AGO61 (Fig. 5a). This indicated that an alternate *O*-Man residue(s) within α-DG373 (other than T317 and T319) was utilized as the LARGE-dependent modification site by the action of AGO61. Based on this result, we hypothesized that AGO61 was a key regulator for the expression of a laminin-binding glycan on a specific *O*-Man residue. To test this, we used Δmucin1-Fc, an α-DG-Fc mutant with only one major LARGE-dependent modification site, Thr-379, as it lacked Arg311 through Ile370[31]. As expected, a T379A mutant of Δmucin1-Fc (Δm1-T379A) barely exhibited any laminin-binding activity even under LARGE-overexpression conditions (Fig. 5b). However, LARGE and AGO61 co-overexpression resulted in the production of an IIH6-positive laminin-binding glycan on Δm1-T379A. Moreover, this effect was not observed with an AGO61 mutant (R158H) and several other dystroglycanopathy-associated gene products, including fukutin and FKRP. This supported our hypothesis that AGO61 was the priming enzyme required for determining candidate sites where a laminin-binding glycan was formed.

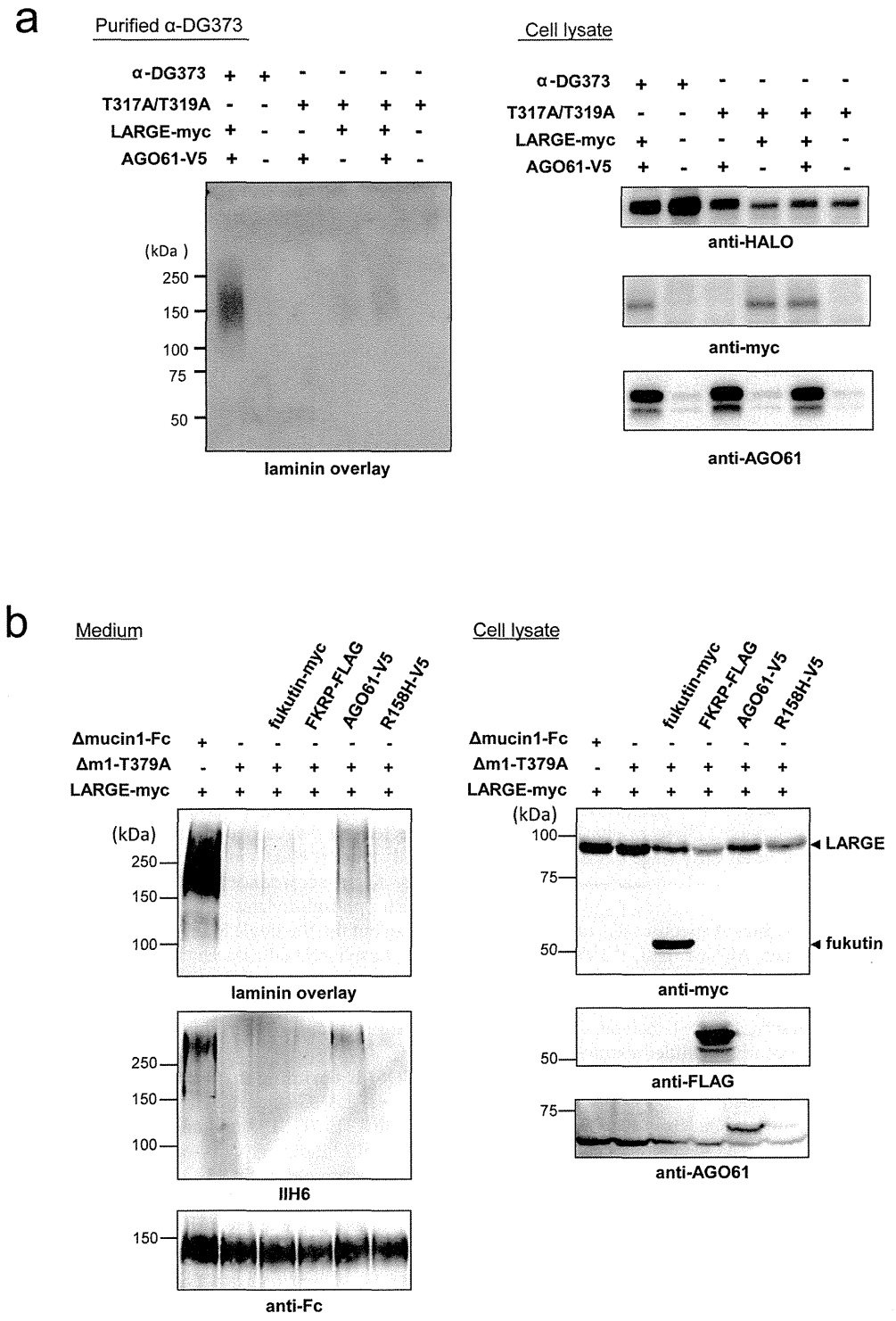

Figure 5 | Laminin-binding glycans are primed by an AGO61-dependent GlcNAc modification. (a) α-DG373-HALO and its mutant T317A/T319A were transiently transfected with or without AOG61 and LARGE-myc into COS7 cells. HALO-fused proteins were collected using HALO resin followed by digestion with TEV protease and then analyzed by laminin overlay. Cell lysates were analyzed for the expression of HALO-fused proteins, LARGE-myc, and AGO61 by Western blot using anti-HALO, anti-myc, and anti-AGO61 antibodies. The full-length blots with anti-HALO, anti-myc, anti-AGO61 antibodies are presented in Supplementary Figs. S7j, S7k, and S7l, respectively. (b) Δmucin1-Fc and Δm1-T379A were transiently transfected with or without fukutin-myc, FKRP-FLAG, AGO61-V5, and AGO61-R158H-mutant-V5 (R158H-V5) into LARGE overexpressing COS1 cells. Secreted proteins were pulled down from the culture medium and analyzed by laminin overlay assay and Western blot using IIH6 and anti-Fc antibodies (medium). Anti-Fc antibody was used to monitor protein loading. Cell lysates were analyzed for the expression of LARGE-myc, fukutin-myc, FKRP-FLAG, and AGO61-V5 by Western blot using anti-myc, anti-FLAG, and anti-AGO61 antibodies. The full-length blots with anti-Fc, anti-FLAG and anti-AGO61 antibodies are presented in Supplementary Figs. S7m, S7n and S7o, respectively.

Discussion

AGO61-KO mice lacked laminin-binding glycans and exhibited phenotypes similar to those of known dystroglycanopathy mutants, as reflected by abnormalities in neural migration and basal lamina formation (Figs. 1 and 2). These defects were also observed in dystroglycanopathy mouse models with mutations of DG, fukutin, B3GNT1, or ISPD, due to a lack of laminin-binding glycans displayed on α-DG[24–26]. Our results show, firstly, that AGO61 is indispensable for the formation of laminin-binding glycans.

Although it has been shown that the laminin-binding glycans of α-DG are extended through a phosphodiester linkage and phosphorylated *O*-Man was identified on recombinant α-DG, their entire structures from the innermost *O*-Man to the outer post-phosphoryl moiety have not been established. It was suggested that the formation of a phosphorylated *O*-mannosyl trisaccharide, GalNAc-β3-GlcNAc-β4-(phosphate-6-)Man, as catalyzed by AGO61, B3GALNT2, and SGK196[21], served as the base for the extension of laminin-binding glycans. More specifically, AGO61 can attach a β-GlcNAc moiety at the 4-position of α-DG-*O*-mannose, which is followed by β3-GalNAc attachment by B3GALNT2 and subsequently SGK196-catalyzed mannose phosphorylation. Our LC-MS/MS data provide the first evidence for the implicated presence of this phosphorylated trisaccharide structure on Thr-317 in the mucin-like region of α-DG, which was previously identified as the formation site of laminin-binding glycans (Fig. 4). In the present study, AGO61-dependent GlcNAc modifications were detected on α-DG-Fc prepared from cell lysates but not in those secreted into the medium irrespective of HFaq treatment (Fig. 3a and Supplementary Fig. S4). These results suggested that additional GalNAc-modifications masked the GlcNAc residues during secretion. The elongation of laminin-binding glycans based on a phosphorylated *O*-mannosyl trisaccharide may be mediated by some uncharacterized glycosyltrasferases encoded for by some dystroglycanopathy-associated genes.

While the mucin-like domain of α-DG possesses numerous serine/threonine residues as potential *O*-mannosylation sites[32–35], AGO61 promotes the GlcNAc modification of *O*-Man at specific sites, as best exemplified by Thr-317 and Thr-319, for the formation of laminin-binding glycans (Fig. 4). Furthermore, in α-DGs mutated at these sites (T317A/T319A-α-DG373 and T379A-Δmucin1-Fc), laminin-binding activity was lost even when LARGE was overexpressed, although it could be rescued solely by overexpressing AGO61. These results indicated that functional α-DG glycosylation was primed by an AGO61-dependent GlcNAc modification.

In summary, we demonstrated that AGO61 served as an essential POMGnT by priming the formation of laminin-binding glycans on α-DG. Our findings provide a critical missing link for understanding the laminin-binding glycan structures displayed on α-DG and provide therapeutic insights for dystroglycanopathy.

Methods

cDNA construction. Expression plasmids for human IgG-Fc fused α-DG (α-DG-Fc) and mouse LARGE fused with myc epitope were constructed as described previously[36]. For the expression plasmid for mouse LARGE fused with HA tag, the cording sequence of mouse LARGE was amplified by PCR and cloned into phCMV3 (Genlantis). For an AGO61 expression vector, the encoding sequence of mouse AGO61 was amplified by PCR and cloned into pcDNA3.1/V5-His-TOPO (C-terminal hexahistidine and V5 tags) (Invitrogen). Amino acid substitutions and deletion mutants of α-DG (α-DG373, α-DG428, and α-DG485) were made using standard PCR and genetic engineering techniques. These mutants were cloned into pFC14K HaloTag CMV Flexi vectors (C-terminal HALO tags) (Promega). For fukutin and FKRP expression vectors, the encoding sequences of mouse fukutin and FKRP were amplified by PCR and cloned into C terminal p3XFLAG-CMV (sigma) and pSecTag2 (Invitrogen), respectively.

Antibodies. We used the following primary antibodies in this study: anti-AGO61 monoclonal antibody (mAb) (Atlas Antibodies AB); anti-*O*-GlcNAc (CTD110.6) mAb (Cell Signaling Technology); anti-*O*-GlcNAc (HGAC85) mAb (Novus Biologicals); anti-Halo mAb (Promega); anti-laminin polyclonal antibody (pAb) (Sigma); anti-Myc mAb and IIH6 mAb (Millipore); anti-HA mAb (Nakalai Tesque); anti-Fc pAb (Jackson ImmunoResearch); anti-β-DG mAb (Novocastra); and α-DG core pAb (goat polyclonal antibody against the C-terminal domain if the a-DG polypeptide)[27]. The following secondary antibodies were used for Western blot analysis: horseradish peroxidase (HRP)-conjugated anti-rabbit IgG mAb (Invitrogen); HRP-conjugated anti-mouse IgM mAb (Thermo Scientific); and HRP-conjugated anti-mouse IgG mAb (Invitrogen).

Generation of AGO61 mutant mice. AGO61 mutants (Acc. No. CDB0628K: http://www.cdb.riken.jp/arg/mutant%20mice%20list.html) were generated as described at http://www.cdb.riken.jp/arg/Methods.html (Fig. S1 in Supporting Information). The described genotypes were consistently observed irrespective of their ES cell clone of origin, number of successive brother–sister mating generations, or backcrossing with C57BL/6J mice (more than 10 generations). PCR genotyping of AGO61 alleles was performed using Ex Taq polymerase (Takara) and the following primers as indicated in Fig. S2 (Supporting Information): an AGO61-specific forward primer (AgoF 5′-GTTGGTGGGCTAGGCAGATA-3′); a neo-specific forward primer (NeoF 5′-TCGCCTTCTTGACGAGTTCT -3′); and a common reverse primer (CoR 5′-CCTCCTGGTTGGATTTGAGA-3′).

Mice. All animal treatments and experiments were done in accordance with the guidelines and regulations of Nagoya City University. The protocol was approved by the Committee for Animal Experiments of the Graduate School of Pharmaceutical Sciences, Nagoya City University.

Cell culture and transfection. Neuro2a, COS1, and COS7 cells were maintained in Dulbecco's modified Eagle's medium (DMEM, Life Technologies) supplemented with 10% fetal bovine serum (FBS) in 5% CO2 at 37°C. For cDNA transfection, cells were grown overnight and transfected using Lipofectamine 2000 (Life Technologies) according to the manufacturer's instructions.

Mouse embryo fibroblasts (MEFs) were prepared from individual AGO61 mutant and wild-type embryos at embryonic day 13.5. An embryo without a head and internal organs was minced and treated with 0.1% trypsin at 37°C for 30 min. These cells were grown and maintained in DMEM containing 10% FBS. Rescue experiments were conducted with AGO KO MEFs using expression vectors for AGO61 and its mutants with loss of function mutations (R158H and R445stop) using an NEPA21 electroporator (NEPA Gene).

Purification of HALO-tag fused proteins. Recombinant α-DG mutants were purified using HaloLink resin (Promega). A HALO-tag was removed by proteolytic cleavage using HaloTEV protease (Promega) according to the manufacturer's instructions. Purified proteins were separated by SDS-PAGE and subjected to silver staining or Western blotting.

Western blotting and laminin overlay. Western blotting and laminin overlay were performed as described previously[36,37].

HFaq treatment. To hydrolyze phosphoester linkages, lysates of brain tissues were treated with ice-cold 48% HFaq (WAKO) at 0°C for 16 h. After removing HFaq with N_2 gas, the resulting lysates were subjected to SDS-PAGE followed by Western blot analysis. After SDS-PAGE, proteins were transferred onto PVDF membranes. The membranes were incubated with ice-cold 48% HFaq at 4°C for 16 h. Control samples were prepared similarly and treated with ice-cold water. The membranes were then washed thrice with ice-cold water to remove residual HF and subjected to laminin overlay assay or immunoblotting.

Glycosidase treatments. Recombinant α-DG was treated with β-*N*-acetylhexosaminidase (New England Biolabs), β-*N*-acetylglucosaminidase (New England Biolabs), or α-*N*-acetylgalactosaminidase (New England Biolabs) according to the manufacturer's instructions. These specimens were subjected to Western blot analysis with an anti-*O*-GlcNAc antibody, CTD110.6.

LC-MS/MS and data analysis. In-gel tryptic digestion of recombinant proteins was performed as previously described[37]. Extracted peptides were solubilized in 0.1% formic acid and analyzed by nanospray LC-MS2 using a nanoACQUITY UPLC System (Waters, Milford, MA, USA) coupled to an LTQ-Orbitrap Velos (Thermo Scientific) through a PicoView (PV550, New Objective, Woburn, MA, USA) nanospray interface. Peptide mixtures were loaded onto a 75 μm × 250 mm nanoACQUITY UPLC BEH130 column packed with C18 resin (Waters, Milford USA) and separated at a flow rate of 300 nl/min using a linear gradient of 5%–50% of solvent B (95% acetonitrile with 0.1% formic acid) in 80 min, followed by a sharp increase to 85% B in 1 min and held at 85% B for another 10 min. Solvent A was 0.1% formic acid in water. The data acquisition cycle included a full MS scan (m/z 400–2000) recorded in the Orbitrap analyzer at 30,000 resolution, followed by data dependent MS2 acquisition of the 20 most intense peptide ions in the linear ion trap. Precursor ion isolation width was set at 3 Th and all singly charged precursors were excluded. The automatic gain control (AGC) targets for Orbitrap full MS and ion trap MSn were set at 1 × 106 and 1 × 104, respectively. All MS/MS raw data were processed using DeconMSn version 2.2.2.2 and directly searched against the α-DG protein sequence using the Mascot Daemon 2.4 server with the following criteria: trypsin digestion; fixed modification set as carbamidomethyl (Cys); variable modifications set as oxidation (Met), Hex (Thr/Ser), HexNAc (Thr/Ser), and PhophoHex (Thr/Ser); up to one missed cleavage allowed; and mass accuracy of

10 ppm for the parent ion and 0.60 Da for fragment ions. Closely eluting glycopeptides corresponding to other glycoforms were further identified manually by inspecting the raw data.

Semi-quantitative RT-PCR. Semi-quantitative RT-PCR was done as described previously[36]. In brief, total RNA was isolated from embryonic brains at embryonic day 17.5 carrying wild-type and mutant genotypes using TRIzol reagent (Life Technologies). cDNAs were synthesized from the total RNAs as templates using SuperScriptIII reverse transcriptase (Life Technologies). To determine mRNA expression levels, PCR was done with the following primer pairs: DAG1: GCCAGATTCGCCCAACACTGACAAT and CCACCCAGGCATCTACCCTGTCAAT; LARGE: GTCAGATGCAGAAGCCCAGCAGTTC and TGGGGAAAGAGAGTCTGTAGCGCAG; LARGE2: CGAGAGCTGCTCACTCTGAT and GGCATCCAAAGAGCTCTCTT; POMGnT1: TCGTGGGACGAAAAGGAGGTCC and TGGGCCGGTTCCCTGCAATG; POMT1: TTGCCCGCATCACCCAAGGC and GGCTGCGACATCGTGCGTGTT; POMT2: TTGCTGGCTACCTGAGCGGG and AGGGGGCAGAGAAAGGCCTGTT; fukutin: CACTATTTGTCTGCAAGGAATGGAC and CTTGCTTTCAGTCTTTAGGCATTGA; FKRP: CTTCTGTCCCGCTTCAGTTC and AACCAGAGAGAGCCCAGTCA; B3gnt1: AATCAGCCAGGCTTGTGAGC and TGGAGGCATGTTTCTTACCCC; ISPD: TGGATCACATAGGCGGAGAC and GCTTCTGCTCATCCTGTGAGT; and GAPDH: GGAAGGGCTCATGACCACAGTCCAT and CATACTTGGCAGGTTTCTCCAGGCG. PCR products were analyzed by agarose gel electrophoresis using 1% agarose gels.

Immunohistochemistry. Mouse embryonic brains at embryonic day 17.5 carrying wild-type and mutated genotypes were fixed in phosphate-buffered saline containing 4% paraformaldehyde, embedded in O.C.T. compound (Sakura Finetechnical, Tokyo, Japan), and frozen in liquid nitrogen. Cryosections (20 μm thick) were prepared from the embedded brains and stained with anti-nestin and anti-laminin antibodies. For a secondary antibody, Alexa Fluor 488-conjugated anti-goat IgG antibody (Life Technologies) or Alexa Fluor 546-conjugated anti-rabbit IgG antibody (Life Technologies) was used. Nuclei were stained with DAPI (1 μg/mL; Sigma-Aldrich). Stained sections were photographed under a Nikon Eclipse TE300 fluorescent microscope (Nikon).

Immunocytochemistry. Neuro2a cells transfected with an AGO expression vector and subcellular localization vectors (pDS-red2-ER or pAcGFP-Golgi; Clontech, Palo Alto, CA) were plated onto chamber slides (Nalge Nunc International) and fixed in PBS containing 4% paraformaldehyde. Cells were treated for 2 h with PBS containing 3% fetal bovine serum and 0.1% Triton X-100, and then stained with primary antibodies, including an anti-AGO61 monoclonal antibody (BD Biosciences, San Jose, CA), and a secondary antibody, an anti-rabbit IgG antibody conjugated with Alexa Fluor 488 or Alexa Fluor 595 (BD Biosciences). Nuclei were stained with 2 μg/mL of Hoechst 33258 (Sigma-Aldrich). Stained cells were photographed under a Nikon Eclipse TE300 fluorescent microscope.

1. Michele, D. E. & Campbell, K. P. Dystrophin-glycoprotein complex: post-translational processing and dystroglycan function. *J. Biol. Chem.* **278**, 15457–60 (2003).
2. Muntoni, F., Torelli, S. & Brockington, M. Muscular dystrophies due to glycosylation defects. *Neurotherapeutics* **5**, 627–32 (2008).
3. Holt, K. H., Crosbie, R. H., Venzke, D. P. & Campbell, K. P. Biosynthesis of dystroglycan: processing of a precursor propeptide. *FEBS Lett.* **468**, 79–83 (2000).
4. Ibraghimov-Beskrovnaya, O. *et al.* Primary structure of dystrophin-associated glycoproteins linking dystrophin to the extracellular matrix. *Nature* **355**, 696–702 (1992).
5. Barresi, R. & Campbell, K. P. Dystroglycan: from biosynthesis to pathogenesis of human disease. *J. Cell Sci.* **119**, 199–207 (2006).
6. Beltran-Valero de Bernabe, D. *et al.* Mutations in the O-mannosyltransferase gene POMT1 give rise to the severe neuronal migration disorder Walker-Warburg syndrome. *Am. J. Hum. Genet.* **71**, 1033–43 (2002).
7. Manya, H. *et al.* Demonstration of mammalian protein *O*-mannosyltransferase activity: coexpression of POMT1 and POMT2 required for enzymatic activity. *Proc. Natl. Acad. Sci. U.S.A.* **101**, 500–5 (2004).
8. van Reeuwijk, J. *et al.* POMT2 mutations cause α-dystroglycan hypoglycosylation and Walker-Warburg syndrome. *J. Med. Genet.* **42**, 907–12 (2005).
9. Yoshida, A. *et al.* Muscular dystrophy and neuronal migration disorder caused by mutations in a glycosyltransferase, POMGnT1. *Dev. Cell* **1**, 717–24 (2001).
10. Carss, K. J. *et al.* Mutations in GDP-mannose pyrophosphorylase B cause congenital and limb-girdle muscular dystrophies associated with hypoglycosylation of α-dystroglycan. *Am. J. Hum. Genet.* **93**, 29–41 (2013).
11. Longman, C. *et al.* Mutations in the human LARGE gene cause MDC1D, a novel form of congenital muscular dystrophy with severe mental retardation and abnormal glycosylation of α-dystroglycan. *Hum. Mol. Genet.* **12**, 2853–61 (2003).
12. Inamori, K. *et al.* Dystroglycan function requires xylosyl- and glucuronyltransferase activities of LARGE. *Science* **335**, 93–6 (2012).
13. Yoshida-Moriguchi, T. *et al.* *O*-mannosyl phosphorylation of α-dystroglycan is required for laminin binding. *Science* **327**, 88–92 (2010).
14. Kobayashi, K. *et al.* An ancient retrotransposal insertion causes Fukuyama-type congenital muscular dystrophy. *Nature* **394**, 388–92 (1998).
15. Brockington, M. *et al.* Mutations in the fukutin-related protein gene (FKRP) cause a form of congenital muscular dystrophy with secondary laminin a2 deficiency and abnormal glycosylation of α-dystroglycan. *Am. J. Hum. Genet.* **69**, 1198–209 (2001).
16. Buysse, K. *et al.* Missense mutations in β-1,3-N-acetylglucosaminyltransferase 1 (B3GNT1) cause Walker-Warburg syndrome. *Hum. Mol. Genet.* **22**, 1746–54 (2013).
17. Roscioli, T. *et al.* Mutations in ISPD cause Walker-Warburg syndrome and defective glycosylation of α-dystroglycan. *Nat. Genet.* **44**, 581–5 (2012).
18. Willer, T. *et al.* ISPD loss-of-function mutations disrupt dystroglycan *O*-mannosylation and cause Walker-Warburg syndrome. *Nat. Genet.* **44**, 575–80 (2012).
19. Vuillaumier-Barrot, S. *et al.* Identification of mutations in TMEM5 and ISPD as a cause of severe cobblestone lissencephaly. *Am. J. Hum. Genet.* **91**, 1135–43 (2012).
20. Manzini, M. C. *et al.* Exome sequencing and functional validation in zebrafish identify GTDC2 mutations as a cause of Walker-Warburg syndrome. *Am. J. Hum. Genet.* **91**, 541–7 (2012).
21. Yoshida-Moriguchi, T. *et al.* SGK196 is a glycosylation-specific *O*-mannose kinase required for dystroglycan function. *Science* **341**, 896–899 (2013).
22. Stevens, E. *et al.* Mutations in B3GALNT2 cause congenital muscular dystrophy and hypoglycosylation of a-dystroglycan. *Am. J. Hum. Genet.* **92**, 354–65 (2013).
23. Jae, L. T. *et al.* Deciphering the glycosylome of dystroglycanopathies using haploid screens for lassa virus entry. *Science* **340**, 479–83 (2013).
24. Chiyonobu, T. *et al.* Effects of fukutin deficiency in the developing mouse brain. *Neuromuscul. Disord.* **15**, 416–26 (2005).
25. Satz, J. S. *et al.* Distinct functions of glial and neuronal dystroglycan in the developing and adult mouse brain. *J. Neurosci.* **30**, 14560–72 (2010).
26. Wright, K. M. *et al.* Dystroglycan organizes axon guidance cue localization and axonal pathfinding. *Neuron* **76**, 931–44 (2012).
27. Kanagawa, M. *et al.* Residual laminin-binding activity and enhanced dystroglycan glycosylation by LARGE in novel model mice to dystroglycanopathy. *Hum. Mol. Genet.* **18**, 621–31 (2009).
28. Yu, M. *et al.* Adeno-associated viral-mediated LARGE gene therapy rescues the muscular dystrophic phenotype in mouse models of dystroglycanopathy. *Hum Gene Ther.* **24**, 317–30 (2013).
29. Isono, T. *O*-GlcNAc-specific antibody CTD110.6 cross-reacts with *N*-GlcNAc2-modified proteins induced under glucose deprivation. *PLoS One* **6**, e18959 (2011).
30. Hara, Y. *et al.* Like-acetylglucosaminyltransferase (LARGE)-dependent modification of dystroglycan at Thr-317/319 is required for laminin binding and arenavirus infection. *Proc. Natl. Acad. Sci. U.S.A.* **108**, 17426–31 (2011).
31. Nakagawa, N., Takematsu, H. & Oka, S. HNK-1 sulfotransferase-dependent sulfation regulating laminin-binding glycans occurs in the post-phosphoryl moiety on α-dystroglycan. *Glycobiology* (2013).
32. Gomez Toledo, A. *et al.* *O*-Mannose and *O*-*N*-acetyl galactosamine glycosylation of mammalian α-dystroglycan is conserved in a region-specific manner. *Glycobiology* **22**, 1413–23 (2012).
33. Stalnaker, S. H. *et al.* Site mapping and characterization of *O*-glycan structures on α-dystroglycan isolated from rabbit skeletal muscle. *J. Biol. Chem.* **285**, 24882–91 (2010).
34. Nilsson, J., Larson, G. & Grahn, A. Characterization of site-specific *O*-glycan structures within the mucin-like domain of α-dystroglycan from human skeletal muscle. *Glycobiology* **20**, 1160–9 (2010).
35. Kuga, A. *et al.* Absence of post-phosphoryl modification in dystroglycanopathy mouse models and wild-type tissues expressing non-laminin binding form of α-dystroglycan. *J. Biol. Chem.* **287**, 9560–7 (2012).
36. Nakagawa, N., Manya, H., Toda, T., Endo, T. & Oka, S. Human natural killer-1 sulfotransferase (HNK-1ST)-induced sulfate transfer regulates laminin-binding glycans on α-dystroglycan. *J. Biol. Chem.* **287**, 30823–32 (2012).
37. Yagi, H. *et al.* HNK-1 epitope-carrying tenascin-C spliced variant regulates the proliferation of mouse embryonic neural stem cells. *J. Biol. Chem.* **285**, 37293–301 (2010).

Acknowledgments

This work was supported by Grants-in-aid for Scientific Research on Innovative Areas [No. 24110512 (to H.Y.) and No. 23110006 (to S.O.), Deciphering sugar chain-based signals regulating integrative neuronal functions and No. 25102008, Dynamical ordering of biomolecular systems for creation of integrated functions (to K.Kato)] and Scientific Research (A) [No. 23249049 (to T.T.) and No. 24249002 (to K.Kato)] from the Japan Society for Promotion of Science (JSPS), and by a Grant-in-aid for JSPS Fellows (No. 252038) (to N.N.). We thank Prof. Ikenaka (National Institute for Physiological Sciences) and Prof. Hattori (Nagoya City Univ.) for technical guidance with immunohistochemistry. We also thank Dr. Kanagawa (Kobe Univ.) for useful discussion for this manuscript. LC-MS/MS data were acquired at the Core Facilities for Protein Structural Analysis at Academia Sinica, supported under the Taiwan National Core Facility Program for Biotechnology (NSC102-2319-B-001-003).

Author contributions

H.Y., S.O., T.T. and K.Kato designed the research; H.K. and T.A. established AGO null mice; H.Y., N.N. and T.S. performed the biochemical exprerimets; H.Y., S.W. and K. Khoo

performed LC-MS/MS analyses; H.Y., S.O., K. Khoo and K. Kato contributed to the conception of this work and wrote the paper.

Additional information

Supplementary information accompanies this paper at http://www.nature.com/scientificreports

Competing financial interests: The authors declare no competing financial interests.

How to cite this article: Yagi, H. *et al.* AGO61-dependent GlcNAc modification primes the formation of functional glycans on α-dystroglycan. *Sci. Rep.* **3**, 3288; DOI:10.1038/srep03288 (2013).

Neurobiology of Aging 35 (2014) 266.e5–266.e14

Contents lists available at ScienceDirect

Neurobiology of Aging

journal homepage: www.elsevier.com/locate/neuaging

The protective effect of LRRK2 p.R1398H on risk of Parkinson's disease is independent of *MAPT* and *SNCA* variants

Michael G. Heckman [a,*], Alexis Elbaz [b,c], Alexandra I. Soto-Ortolaza [d], Daniel J. Serie [a], Jan O. Aasly [e], Grazia Annesi [f], Georg Auburger [g], Justin A. Bacon [d], Magdalena Boczarska-Jedynak [h], Maria Bozi [i], Laura Brighina [j], Marie-Christine Chartier-Harlin [k,l], Efthimios Dardiotis [m,n], Alain Destée [k,l,o], Carlo Ferrarese [j], Alessandro Ferraris [p], Brian Fiske [q], Suzana Gispert [g], Georgios M. Hadjigeorgiou [m,n], Nobutaka Hattori [r], John P.A. Ioannidis [s,t], Barbara Jasinska-Myga [h], Beom S. Jeon [u], Yun Joong Kim [v], Christine Klein [w], Rejko Kruger [x], Elli Kyratzi [y], Chin-Hsien Lin [z], Katja Lohmann [w], Marie-Anne Loriot [aa,bb,cc], Timothy Lynch [dd], George D. Mellick [ee], Eugénie Mutez [k,l,ff], Grzegorz Opala [h], Sung Sup Park [gg], Simona Petrucci [p], Aldo Quattrone [hh], Manu Sharma [x,ii], Peter A. Silburn [jj], Young Ho Sohn [kk], Leonidas Stefanis [y], Vera Tadic [w], Hiroyuki Tomiyama [r], Ryan J. Uitti [ll], Enza Maria Valente [p,mm], Demetrios K. Vassilatis [y], Carles Vilariño-Güell [nn], Linda R. White [oo], Karin Wirdefeldt [pp], Zbigniew K. Wszolek [ll], Ruey-Meei Wu [qq], Georgia Xiromerisiou [m,n], Demetrius M. Maraganore [rr], Matthew J. Farrer [nn], Owen A. Ross [d,**], on behalf of the Genetic Epidemiology Of Parkinson's Disease (GEO-PD) Consortium

[a] *Section of Biostatistics, Mayo Clinic, Jacksonville, FL, USA*
[b] *INSERM, Centre for research in Epidemiology and Population Health, U1018, Social and Occupational Determinants of Health, Villejuif, France*
[c] *University of Versailles St-Quentin, UMRS 1018, Villejuif, France*
[d] *Department of Neuroscience, Mayo Clinic, Jacksonville, FL, USA*
[e] *Department of Neuroscience, Norwegian University of Science and Technology, Trondheim, Norway*
[f] *Institute of Neurological Sciences, National Research Council, Cosenza, Italy*
[g] *Department of Neurology, Goethe University, Frankfurt am Main, Germany*
[h] *Department of Neurology, Medical University of Silesia, Katowice, Poland*
[i] *General Hospital of Syros, Syros, Greece*
[j] *Department of Neuroscience-Section of Neurology, University of Milano-Bicocca, San Gerardo Hospital, Monza, Italy*
[k] *Centre de Recherche Jean-Pierre Aubert, University Lille Nord de France, Lille, France*
[l] *INSERM, U837, Lille, France*
[m] *Department of Neurology, Laboratory of Neurogenetics, Faculty of Medicine, University of Thessaly, Larissa, Greece*
[n] *Laboratory of Neurogenetics, Biomedicine Department, CERETETH, Larissa, Greece*
[o] *University Hospital, CHRU, Lille, France*
[p] *IRCCS Casa Sollievo della Sofferenza, CSS-Mendel Laboratory, San Giovanni Rotondo, Italy*
[q] *The Michael J Fox Foundation for Parkinson's Research, New York, NY, USA*
[r] *Department of Neurology, Juntendo University School of Medicine, Tokyo, Japan*
[s] *Clinical and Molecular Epidemiology Unit, Department of Hygiene and Epidemiology, University of Ioannina Medical School, Ioannina, Greece*
[t] *Stanford Prevention Research Center, Stanford University School of Medicine, Stanford, CA, USA*
[u] *Department of Neurology, Seoul National University Hospital, Seoul, South Korea*
[v] *ILSONG Institute of Life Science and Department of Neurology, Hallym University, Anyang, South Korea*
[w] *Institute of Neurogenetics, University of Luebeck, Luebeck, Germany*
[x] *Department for Neurodegenerative Diseases, Hertie-Institute for Clinical Brain Research and German Center for Neurodegenerative Diseases (DZNE), University of Tübingen, Tübingen, Germany*
[y] *Divisions of Basic Neurosciences and Cell Biology, Biomedical Research Foundation of the Academy of Athens, Athens, Greece*
[z] *Department of Neurology, National Taiwan University Hospital Yun-Lin Branch, Yun-Lin, Taiwan*
[aa] *INSERM, UMR-S 775, Molecular Basis of Response to Xenobiotics, Paris, France*
[bb] *University Paris Descartes, Paris, France*
[cc] *Department of Biochemistry, Pharmacogenetics and Molecular Oncology, Assistance-Publique Hôpitaux de Paris, Georges Pompidou European Hospital (HEGP), Paris, France*
[dd] *Dublin Neurological Institute at the Mater Misericordiae University Hospital, and Conway Institute of Biomolecular and Biomedical Research, University College Dublin, Dublin, Ireland*
[ee] *Eskitis Institute for Cell and Molecular Therapies, Griffith University, Queensland, Australia*

* Corresponding author at: Section of Biostatistics, Mayo Clinic Jacksonville, 4500 San Pablo Road, Jacksonville, FL 32224, USA. Tel.: +1 904 953 1049; fax: +1 904 953 0277.
** Corresponding author at: Department of Neuroscience, Mayo Clinic Jacksonville, 4500 San Pablo Road, Jacksonville, FL 32224, USA. Tel.: +1 904 953 6280; fax: +1 904 953 7370.
E-mail addresses: heckman.michael@mayo.edu (M.G. Heckman), ross.owen@mayo.edu (O.A. Ross).

0197-4580/$ – see front matter
http://dx.doi.org/10.1016/j.neurobiolaging.2013.07.013

[ff] Centre Hospitalier Regional Universitaire de Lille, Lille, France
[gg] Department of Laboratory Medicine, Seoul National University Hospital, Seoul, South Korea
[hh] Department of Medical Sciences, Institute of Neurology, University Magna Graecia, and Neuroimaging Research Unit, National Research Council, Catanzaro, Italy
[ii] Institute for Clinical Epidemiology and Applied Biometry, University of Tübingen, Tübingen, Germany
[jj] Centre for Clinical Research, Royal Brisbane Hospital, University of Queensland, Australia
[kk] Department of Neurology, Yonsei University College of Medicine, Seoul, South Korea
[ll] Department of Neurology, Mayo Clinic, Jacksonville, FL, USA
[mm] Department of Medicine and Surgery, University of Salerno, Salerno, Italy
[nn] Department of Medical Genetics, University of British Columbia, Vancouver, Canada
[oo] University Hospital and Norwegian University of Science and Technology, Trondheim, Norway
[pp] Department of Clinical Neuroscience and Department of Medical Epidemiology and Biostatistics, Karolinska Institutet, Stockholm, Sweden
[qq] Department of Neurology, National Taiwan University Hospital, College of Medicine, National Taiwan University, Taipei, Taiwan
[rr] Department of Neurology, North Shore University Health System, Evanston, IL, USA

ARTICLE INFO

Article history:
Received 9 April 2013
Received in revised form 10 July 2013
Accepted 15 July 2013
Available online 17 August 2013

Keywords:
Parkinson's disease
LRRK2
SNCA
MAPT
Interaction
Genetics

ABSTRACT

The best validated susceptibility variants for Parkinson's disease are located in the α-synuclein (*SNCA*) and microtubule-associated protein tau (*MAPT*) genes. Recently, a protective p.N551K-R1398H-K1423K haplotype in the leucine-rich repeat kinase 2 (*LRRK2*) gene was identified, with p.R1398H appearing to be the most likely functional variant. To date, the consistency of the protective effect of LRRK2 p.R1398H across *MAPT* and *SNCA* variant genotypes has not been assessed. To address this, we examined 4 *SNCA* variants (rs181489, rs356219, rs11931074, and rs2583988), the *MAPT* H1-haplotype–defining variant rs1052553, and LRRK2 p.R1398H (rs7133914) in Caucasian (n = 10,322) and Asian (n = 2289) series. There was no evidence of an interaction of LRRK2 p.R1398H with *MAPT* or *SNCA* variants (all $p \geq 0.10$); the protective effect of p.R1398H was observed at similar magnitude across *MAPT* and *SNCA* genotypes, and the risk effects of *MAPT* and *SNCA* variants were observed consistently for LRRK2 p.R1398H genotypes. Our results indicate that the association of LRRK2 p.R1398H with Parkinson's disease is independent of *SNCA* and *MAPT* variants, and vice versa, in Caucasian and Asian populations.

1. Introduction

With an estimated prevalence of between 1% and 2% in individuals more than 65 years of age, Parkinson's disease (PD) is one of the most common age-related neurodegenerative disorders (de Lau and Breteler, 2006; Postuma and Montplaisir, 2009). Long thought of as a sporadic disease, PD now has a well-established genetic component that includes both disease-causing mutations as well as risk-modifying susceptibility variants (Gasser et al., 2011). Of the PD susceptibility variants that have been identified thus far, the best validated have involved those located in the α-synuclein (*SNCA*) gene, which also contains several pathogenic mutations that are linked to familial PD, and in the microtubule-associated protein tau (*MAPT*) gene (Gasser et al., 2011). More specifically, associations with PD have been identified in both Caucasian and Asian populations at the 3′ and 5′ ends of the *SNCA* gene (Mizuta et al., 2006; Mueller et al., 2005; Pankratz et al., 2009; Ross et al., 2007; Satake et al., 2009; Simón-Sánchez et al., 2009; Winkler et al., 2007), whereas the H1 haplotype in *MAPT* is associated with PD in Caucasians but not in Asians, owing to the almost complete absence of the H2 haplotype in the latter group (Evans et al., 2004; Healy et al., 2004; Skipper et al., 2004; Tobin et al., 2008; Wider et al., 2010).

Variation in the leucine-rich repeat kinase 2 (*LRRK2*) gene, which like *SNCA* harbors disease-causing mutations of its own has also been associated with susceptibility to PD in both Caucasian and Asian populations. The majority of proposed *LRRK2* PD risk variants have been relatively rare (minor allele frequencies [MAFs] between 1% and 5%) and have included p.G2385R and p.R1628P in Asian populations as well as the more recently identified p.A419V (in Asians), and p.M1646T (in Caucasians) (Di Fonzo et al., 2006; Farrer et al., 2007; Ross et al., 2008, 2011; Tan et al., 2010). The most common *LRRK2* PD risk factor to date, identified by several groups including our own, has involved a 3-variant (p.N551K-R1398H-K1423K) protective haplotype in both populations (Ross et al., 2011; Tan et al., 2010). It has been shown that the p.1398H variant has reduced kinase activity in comparison to the wild-type p.R1398 (Tan et al. 2010). Given these data, the p.R1398H (rs7133914) substitution, which occurs with a MAF of approximately 7% in Caucasians and 10% in Asians (Heckman et al., in press; Tan et al., 2010), is the most likely functional variant on the haplotype. The protective effect of p.R1398H appears to be strongest in Asians, in whom consistent odds ratios of 0.75 and 0.73 have been observed in studies by Tan et al. (2010) and Ross et al. (2011), with a similar odds ratio of 0.79 observed in a smaller study by Chen et al. (2011). In Caucasians, the odds ratio for p.R1398H observed in the aforementioned study by Ross et al. in a series of 6995 patients and 5595 control subjects was 0.89. This is very similar to the findings of a large meta-analysis of genome-wide association studies, in which, albeit not nominally significant, LRRK2 p.R1398H (MAF ~ 6.7%) had a protective odds ratio of 0.92 and 95% confidence limits ranging from 0.83 to 1.02 in regard to susceptibility to PD (Nalls et al., 2011; personal communication).

To best determine risk of PD for a given individual and to elucidate potential future therapeutic implications, it is important not only to identify individual genetic risk factors but also to understand how these risk factors interact with one another. However, sample sizes needed to reasonably evaluate evidence of such gene–gene interactions are usually fairly large and can be difficult to achieve. This is because the risk factor of interest in an interaction study (presence of the genotype of interest for both variants) occurs much less frequently than the genotype for the individual variants, which can result in a lack of precision in estimated interaction effects. Collaboration between members of the Genetic Epidemiology of Parkinson's Disease (GEO-PD) Consortium and the resulting large number of patients with PD and controls offers the opportunity to effectively examine how recognized susceptibility variants for PD may or may not interact with one another. Such a study was previously undertaken by the GEO-PD Consortium, in which *SNCA* and *MAPT* variants were

examined in relation to risk of PD and found to have independent effects (Elbaz et al., 2011). The identification of PD susceptibility variants in *LRRK2* raises the question of whether the effects of these variants may be modified by those in *SNCA* or *MAPT*, or vice versa. The aim of this study was to evaluate the interaction of the common *LRRK2* susceptibility variant p.R1398H with *SNCA* and *MAPT* variants in relation to risk of PD using Caucasian and Asian patient–control subject series obtained through the GEO-PD Consortium.

2. Methods

2.1. Subjects

As of 2013, the GEO-PD Consortium includes 57 sites from 29 countries and 6 continents that have agreed to share DNA and data for 38,686 patients with PD and 34,871 control subjects (http://www.geopd.org/). A total of 20 sites participating in the GEO-PD Consortium provided data to be used in the current study as part of a project initiated in 2009. The majority of the Caucasian subjects used in this study were also included in the previously mentioned GEO-PD *SNCA-MAPT* interaction study (Elbaz et al., 2011), and the subjects included in this study are a subset of those included in the previously referred to investigation of *LRRK2* exonic variants in relation to PD (Ross et al., 2011). To be consistent with the association analysis in the latter study involving *LRRK2* exonic variants, carriers of *LRRK2* pathogenic variants (n = 64) were excluded. Subjects were not genotyped for known pathogenic *SNCA* mutations and therefore this was not part of our exclusion criteria. In total, 7342 patients with PD and 5269 control subjects from 13 different countries on 4 continents were studied. These subjects were divided into a Caucasian series (5991 patients with PD, 4331 controls, 16 sites, 10 countries) and an Asian series (1351 patients with PD, 938 controls, 4 sites, 3 countries). Table 1 provides demographic information for the Caucasian and Asians series, whereas site-specific information is displayed in Supplementary Table 1.

Patients were diagnosed with PD using standard criteria (Bower et al., 1999; Gelb et al., 1999; Hughes et al., 1992). Controls were individuals free of PD or a related movement disorder at the time of examination. All subjects were unrelated within and between diagnosis groups. The Mayo Clinic Institutional Review Board approved the study; each individual site received local institutional review board approval, and all subjects provided informed consent.

2.2. Genetic analysis

Four *SNCA* variants (3′ end of gene: rs181489, rs356219, rs11931074; 5′ end of gene: rs2583988) as well as the *MAPT* H1-haplotype defining variant rs1052553 were genotyped because of consistently replicated associations with PD (Healy et al., 2004; Mueller et al., 2005; Mizuta et al., 2006; Pankratz et al., 2009; Ross et al., 2007; Satake et al., 2009; Skipper et al., 2004; Simón-Sánchez et al., 2009; Tobin et al., 2008; Wider et al., 2010; Winkler et al., 2007). These 5 variants were chosen for the aforementioned GEO-PD *SNCA-MAPT* interaction study (Elbaz et al., 2011). The REP1 polymorphism located in the *SNCA* promoter has also been associated with PD (Krüger et al., 1999; Maraganore et al., 2006); however, because the 263-bp allele (which has shown the strongest association with PD) is relatively rare, we did not evaluate REP1 in the current study. The *LRRK2* variant rs7133914 (p.R1398H) was also selected for inclusion because of the aforementioned findings demonstrating that is the most likely functional variant on a 3-variant haplotype (all 3 variants in strong linkage disequilibrium with $r^2 > 0.84$ in controls) that affects risk of PD in a protective manner (Ross et al., 2011; Tan et al., 2010).

Table 1
Subject characteristics for the Caucasian and Asian series

Variable	Patients with PD	Controls
Caucasian series	n = 5991	n = 4331
Age, y	69 ± 11 (18–106)	65 ± 15 (21–107)
Gender		
Male	3453 (58%)	2045 (47%)
Female	2538 (42%)	2286 (53%)
Age at onset, y	59 ± 12 (18–96)	NA
Asian series	n = 1351	n = 938
Age, y	61 ± 12 (20–91)	60 ± 11 (23–89)
Gender		
Male	672 (50%)	322 (34%)
Female	679 (50%)	616 (66%)
Age at onset, y	54 ± 12 (20–89)	NA

Sample mean ± SD (minimum–maximum) is given for age of subjects and age at onset. Information was unavailable regarding age in the Caucasian series (147 patients with PD, 21 controls) and Asian series (371 patients with PD, 298 controls). Information was unavailable regarding age at onset in the Caucasian series (723 patients) and Asian series (8 patients).
Key: NA, not applicable; PD, Parkinson's disease; SD, standard deviation.

DNA was sourced from blood and was stored in a freezer at −80 °C. All samples were de-identified with an anonymous code from each site and only a minimal clinical dataset. All *LRRK2* and *SNCA* genotyping was done using MassArray iPLEX chemistry and analyzed using Typer 4.0 (Sequenom, San Diego, CA). *MAPT* rs1052553 was genotyped using an ABI Taqman genotyping assay on an ABI 7900HT Fast Real-Time PCR system and analyzed using SDS 2.2.2 software (Applied Biosystems, Foster City, CA). All genotyping was performed at the Mayo Clinic Florida neurogenetics laboratory (Jacksonville, FL). Primer sequences are provided in Supplementary Table 2 for all variants except for *MAPT* rs1052553. Positive control DNA was run for each variant. Call rates in each series were >95%. There was no evidence of departure from Hardy–Weinberg equilibrium in controls for any of the sites (all $p > 0.05$ after Bonferroni correction).

2.3. Statistical analysis

All analysis was performed separately for the Caucasian and Asian series. Associations of individual *SNCA* variants, *MAPT* rs1052553, and LRRK2 p.R1398H with PD, and pairwise interactions of LRRK2 p.R1398H with *SNCA* and *MAPT* variants in relation to PD, were evaluated using odds ratios (ORs) and 95% confidence intervals (CIs) from fixed-effects logistic regression models adjusted for site. Interactions were evaluated on a multiplicative scale only because it has been shown that when at least one of the interacting factors is protective, biological interactions are expected to result in departure from multiplicative effects (Weinberg, 1986).

We considered LRRK2 p.R1398H under a dominant model (presence vs. absence of the minor allele) in all analyses owing to the very small number of homozygotes of the minor allele, whereas *SNCA* variants were evaluated under an additive model (effect of each additional minor allele), dominant model, recessive model (presence of 2 copies vs. 0 or 1 copy of the minor allele) and genotype model (general comparison across genotypes). *MAPT* rs1052553 was also evaluated under additive, dominant, recessive, and genotype models, but with effects corresponding to the major allele to be consistent with previous reports in which ORs correspond to the H1 risk allele. In Caucasians, 3-gene interactions were also examined. Sensitivity of results to model adjustment for age and gender and to the use of random-effects models (DerSimonian and Laird, 1986) were also assessed when evaluating interactions.

Between-site heterogeneity in interaction ORs was examined using χ^2 tests based on the Q statistic, and also by estimating the I^2 statistic, which measures the proportion of variation in interaction ORs between sites due to heterogeneity beyond chance (Higgins and Thompson, 2002).

A relatively large number of statistical tests of gene–gene interaction were performed in our analyses (24 in the Caucasian series and 8 in the Asian series). To adjust for multiple testing and to control the family-wise error rate at 5%, we used a Bonferroni correction separately for each series, after which p values $\leq$0.0021 (Caucasian series) and $\leq$0.00625 (Asian series) were considered as statistically significant. All statistical analyses were performed using R Statistical Software (version 2.14.0; R Foundation for Statistical Computing, Vienna, Austria).

3. Results

A summary of allele and genotype frequencies for *SNCA* variants, *MAPT* rs1052553, and LRRK2 p.R1398H in our Caucasian and Asian patient-control series is provided in Supplementary Table 3, along with country-specific frequencies. The *SNCA* variants rs181489 and rs2583988 as well as *MAPT* rs1052553 were observed extremely rarely in Asian patients and controls and, as such, were not assessed in association analysis. *SNCA* variants were in relatively weak linkage disequilibrium in controls ($r^2 \leq 0.32$) with the exception of rs181489 and rs356219 in the Caucasian series ($r^2 = 0.58$), rs181489 and rs2583988 in the Caucasian series ($r^2 = 0.53$), and rs356219 and rs11931074 in the Asian series ($r^2 = 0.97$).

To best interpret the results of gene–gene interaction analysis, it is helpful to first understand the effects of individual variants on risk of PD, and therefore single-variant associations with PD for the *SNCA*, *MAPT*, and *LRRK2* variants, which have largely been reported before in the aforementioned GEO-PD studies (Elbaz et al., 2011; Ross et al., 2011), are displayed in Supplementary Table 4. As has been previously shown, all variants were significantly associated with PD.

Evaluations of pairwise interactions of LRRK2 p.R1398H with *SNCA* variants and *MAPT* rs1052553 in relation to PD for the Caucasian series are shown in Table 2. To simplify our presentation of interaction results, we have focused on additive and genotype models for *SNCA* and *MAPT* variants in Table 2, because all of these variants had the strongest association with PD under an additive model except *SNCA* rs11931074 (which was also strongly associated with PD under an additive model), and because genotype models allow for the most general test of interaction. Gene–gene interactions under dominant and

Table 2
Interactions of LRRK2 p.R1398H with *SNCA* and *MAPT* variants in regard to susceptibility to Parkinson's disease (PD) in the Caucasian series under additive and genotype models

Variant/genotype	LRRK2 p.R1398H	Sample genotype count and frequency	Test of association		Test of interaction
			OR (95% CI)	p value	
SNCA rs181489					
CC	GG	3908 (39.9%)	1.00 (reference)	NA	Additive model
CC	GA or AA	599 (6.1%)	0.82 (0.69–0.98)	0.030	OR = 1.06
CT	GG	3636 (37.1%)	1.14 (1.04–1.25)	0.0070	95% CI = 0.88–1.28
CT	GA or AA	542 (5.5%)	1.08 (0.90–1.30)	0.42	p = 0.52
TT	GG	967 (9.9%)	1.65 (1.42–1.92)	1.4E-10	Genotype model[a]
TT	GA or AA	136 (1.4%)	1.40 (0.98–2.00)	0.066	p = 0.14
SNCA rs356219					
AA	GG	3087 (30.9%)	1.00 (reference)	NA	Additive model
AA	GA or AA	440 (4.4%)	0.82 (0.67–1.01)	0.060	OR = 0.98
AG	GG	4142 (41.5%)	1.15 (1.04–1.26)	0.0060	95% CI = 0.82–1.17
AG	GA or AA	628 (6.3%)	1.11 (0.93–1.32)	0.27	p = 0.81
GG	GG	1476 (14.8%)	1.51 (1.33–1.73)	7.2E-10	Genotype model[a]
GG	GA or AA	219 (2.2%)	1.10 (0.83–1.46)	0.51	p = 0.32
SNCA rs11931074					
GG	GG	7443 (74.6%)	1.00 (reference)	NA	Additive model
GG	GA or AA	1061 (10.5%)	0.85 (0.74–0.97)	0.017	OR = 1.06
GT	GG	1300 (12.9%)	1.34 (1.18–1.51)	6.8E-6	95% CI = 0.79–1.43
GT	GA or AA	232 (2.3%)	1.32 (1.00–1.74)	0.052	p = 0.69
TT	GG	59 (0.6%)	1.46 (0.84–2.62)	0.19	Genotype model[a]
TT	GA or AA	12 (0.1%)	0.67 (0.20–2.24)	0.51	p = 0.61
SNCA rs2583988					
CC	GG	4495 (44.6%)	1.00 (reference)	NA	Additive model
CC	GA or AA	677 (6.7%)	0.82 (0.69–0.97)	0.019	OR = 1.07
CT	GG	3480 (34.6%)	1.20 (1.09–1.31)	0.0001	95% CI = 0.89–1.29
CT	GA or AA	500 (5.0%)	1.13 (0.93–1.37)	0.23	p = 0.47
TT	GG	800 (7.9%)	1.42 (1.21–1.67)	1.9E-5	Genotype model[a]
TT	GA or AA	117 (1.2%)	1.22 (0.84–1.80)	0.30	p = 0.56
MAPT rs1052553[b]					
GG	GG	364 (3.6%)	1.00 (reference)	NA	Additive model
GG	GA or AA	58 (0.6%)	0.54 (0.30–0.97)	0.041	OR = 1.05
GA	GG	2617 (25.7%)	1.10 (0.88–1.38)	0.41	95% CI = 0.85–1.30
GA	GA or AA	398 (3.9%)	1.05 (0.78–1.41)	0.75	p = 0.65
AA	GG	5881 (58.0%)	1.36 (1.10–1.70)	0.0055	Genotype model[a]
AA	GA or AA	858 (8.4%)	1.19 (0.92–1.53)	0.19	p = 0.29

ORs and P values result from fixed-effects logistic regression models. For tests of association, the 2 given variants were combined into 1 variable, and the model was adjusted for site. For tests of interaction, models included each of the 2 variants, their interaction, and site. Additive models and genotype models refer to the characterization of *SNCA* and *MAPT* variants; only dominant models were considered for LRRK2 p.R1398H because of the small number of rare homozygotes for this variant. Interaction ORs under an additive model are interpreted as the multiplicative increase in the effect of the minor allele for LRRK2 p.R1398H on PD corresponding to each additional risk allele for *SNCA* and *MAPT* variants, or alternatively as the multiplicative increase in the effect of each additional risk allele for *SNCA* and *MAPT* variants on PD corresponding to presence of the minor allele for LRRK2 p.R1398H.

Key: CI, confidence interval; OR, odds ratio.

[a] Tests of interaction under a genotype model do not produce a single interaction OR, and therefore only a P value is given.

[b] The A allele for *MAPT* rs1052553 corresponds to the H1 haplotype.

recessive models for *SNCA* and *MAPT* variants are shown in Supplementary Tables 5 and 6. In site-adjusted analyses, no interactions of LRRK2 p.R1398H with *SNCA* and *MAPT* variants approached significance after multiple testing adjustment under any statistical model (all interaction $p \geq 0.10$); the protective effect of p.R1398H on risk of PD observed in similar magnitude for different genotypes of *SNCA* and *MAPT* variants, whereas the risk effects of *SNCA* and *MAPT* variants were seen similarly for subjects with and without a copy of the minor allele for p.R1398H. All interaction ORs were close to 1.0 in magnitude indicating lack of any interaction with LRRK2 p.R1398H, the only exceptions involving rare genotypes for *MAPT* rs1052553 under a dominant model (Supplementary Table 5) and *SNCA* rs11931074 under a recessive model (Supplementary Table 6), which are best interpreted with caution owing to the non-significant interactions and very low genotype frequencies. The lack of interaction of LRRK2 p.R1398H with *MAPT* and *SNCA* variants was also observed when adjusting for age and gender (Supplementary Table 7) in those subjects with that information available (98%) and also when using a random effects model (Supplementary Table 8). Results of country-specific interaction analysis are shown in Supplementary Table 9. Between-site heterogeneity regarding interactions with LRRK2 p.R1398H was low for *SNCA* rs356219, rs11931074, and rs2583988 ($I^2 = 0\%$, $p \geq 0.45$) and moderate for *SNCA* rs181489 and *MAPT* rs1052553 ($I^2 = 25\%$–36%, $p \geq 0.075$) (Supplementary Table 8).

More detailed analysis combining genotypes across all 3 genes for *SNCA* variants, *MAPT* rs1052553, and LRRK2 p.R1398H in the Caucasian series is displayed in Supplementary Table 10 and Fig. 1, where rare homozygotes were collapsed with heterozygotes for each variant to avoid extremely rare 3-variant genotype combinations. There was no evidence of any interaction in these 3-gene analyses (all, $p \geq 0.63$).

Interactions of LRRK2 p.R1398H with *SNCA* variants rs356219 and rs11931074 in the Asian series are examined in Table 3 in analyses adjusted for site. Individual effects of LRRK2 p.R1398H and *SNCA* variants on risk of PD were observed consistently across variants in the other gene, with no statistically significant evidence of gene–gene interaction (all interaction, $p \geq 0.14$). All interaction ORs were between 1.17 and 1.39, indicating a slight but nonsignificant reduction of the protective effect of LRRK2 p.R1398H on risk of PD when the risk allele for *SNCA* variants was present, and a similar small and nonsignificant enhancement of the *SNCA* risk effects, given the protective genotype for p.R1398H (Fig. 2). Results were similar when adjusting for age and gender (Supplementary Table 7) in the

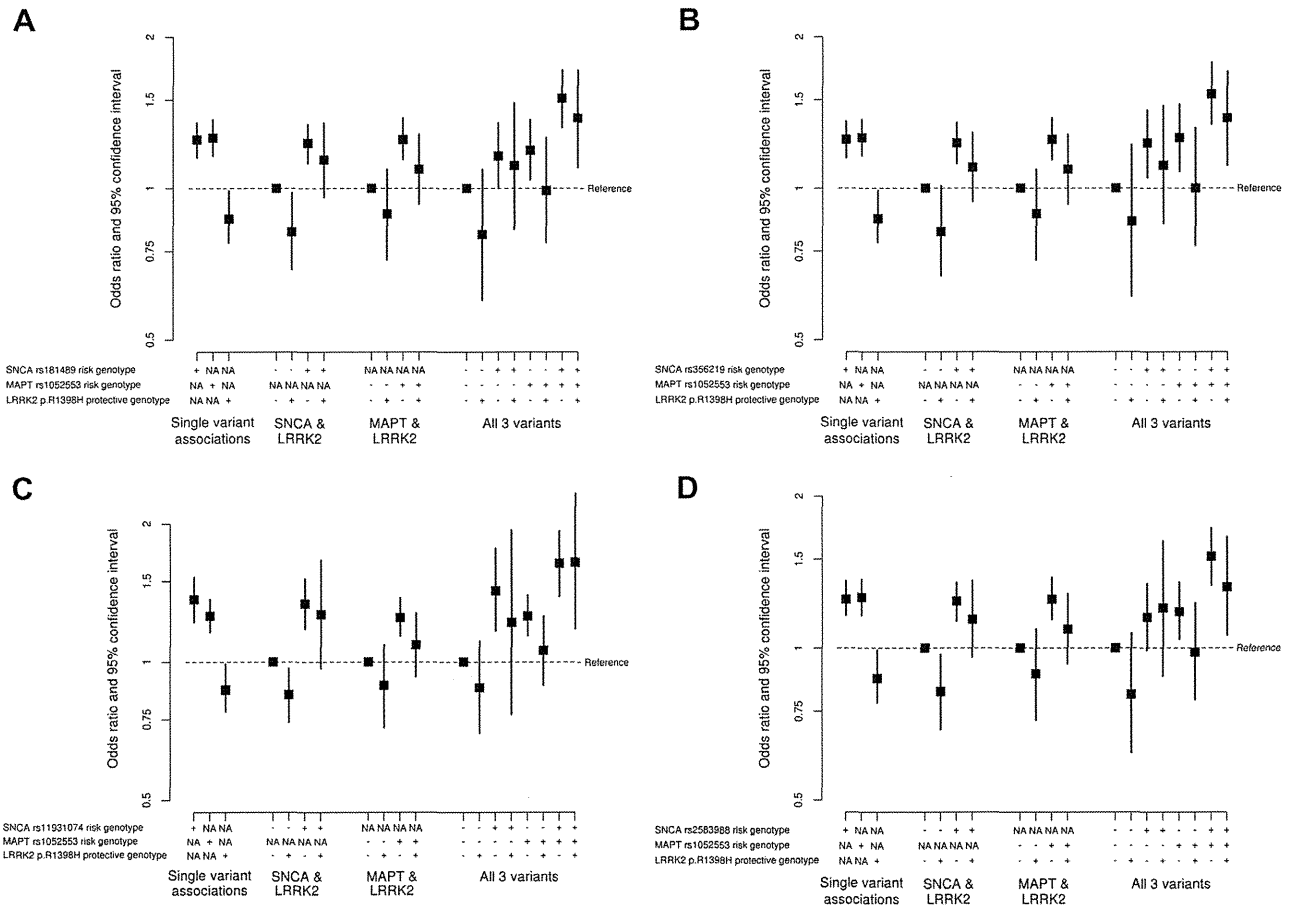

Fig. 1. (A) Individual and combined effects of *SNCA* rs181489, *MAPT* rs1052553, and LRRK2 p.R1398H on risk of Parkinson's disease (PD) in the Caucasian series. For *SNCA* rs181489, the risk genotype was CT or TT (i.e., presence of the minor allele). (B) Individual and combined effects of *SNCA* rs356129, *MAPT* rs1052553, and LRRK2 p.R1398H on risk of PD in the Caucasian series. For *SNCA* rs356129, the risk genotype was AG or GG (i.e., presence of the minor allele). (C) Individual and combined effects of *SNCA* rs11931074, *MAPT* rs1052553, and LRRK2 p.R1398H on risk of PD in the Caucasian series. For *SNCA* rs11931074, the risk genotype was GT or TT (i.e., presence of the minor allele). (D) Individual and combined effects of *SNCA* rs2583988, *MAPT* rs1052553, and LRRK2 p.R1398H on risk of PD in the Caucasian series. For *SNCA* rs2583988, the risk genotype was CT or TT (i.e., presence of the minor allele). (A–D) For *MAPT* rs1052553, the risk genotype was AA (i.e., presence of 2 copies of the major allele); for LRRK2 p.R1398H, the protective genotype was GA or AA (i.e., presence of the minor allele). NA indicates that a given SNP was not involved in the particular portion of the analysis.

Table 3
Interactions of LRRK2 p.R1398H with *SNCA* variants in regard to susceptibility to Parkinson's disease (PD) in the Asian series

Variant/genotype	LRRK2 p.R1398H	Sample genotype count and frequency	Test of association		Test of interaction
			OR (95% CI)	*p* value	
Additive/genotype models[a]					
SNCA rs356219					
AA	GG	282 (12.9%)	1.00 (reference)	N/A	Additive model
AA	GA or AA	83 (3.8%)	0.64 (0.39–1.06)	0.087	OR = 1.17
AG	GG	808 (37.0%)	1.59 (1.21–2.09)	0.0009	95% CI = 0.87–1.59
AG	GA or AA	232 (10.6%)	1.19 (0.84–1.69)	0.33	*p* = 0.30
GG	GG	623 (28.5%)	2.09 (1.56–2.79)	6E-7	Genotype model[d]
GG	GA or AA	156 (7.1%)	1.84 (1.23–2.77)	0.0031	*p* = 0.59
SNCA rs11931074					
GG	GG	302 (13.3%)	1.00 (reference)	N/A	Additive model
GG	GA or AA	89 (3.9%)	0.61 (0.37–0.98)	0.044	OR = 1.25
GT	GG	843 (37.2%)	1.55 (1.19–2.02)	0.0012	95% CI = 0.93–1.69
GT	GA or AA	243 (10.7%)	1.06 (0.75–1.49)	0.75	*p* = 0.14
TT	GG	630 (27.8%)	1.90 (1.43–2.51)	7.8E-6	Genotype model[d]
TT	GA or AA	158 (7.0%)	1.75 (1.18–2.61)	0.0059	*p* = 0.31
Dominant model[b]					
SNCA rs356219					
AA	GG	282 (12.9%)	1.00 (reference)	N/A	OR = 1.23
AA	GA or AA	83 (3.8%)	0.64 (0.39–1.06)	0.087	95% CI = 0.71–2.14
AG or GG	GG	1431 (65.5%)	1.78 (1.38–2.31)	1.10E-5	*p* = 0.47
AG or GG	GA or AA	388 (17.8%)	1.41 (1.03–1.92)	0.030	
SNCA rs11931074					
GG	GG	302 (13.3%)	1.00 (reference)	N/A	OR = 1.25
GG	GA or AA	89 (3.9%)	0.61 (0.37–0.98)	0.043	95% CI = 0.74–2.15
GT or TT	GG	1473 (65.0%)	1.69 (1.31–2.17)	4.3E-5	*p* = 0.41
GT or TT	GA or AA	401 (17.7%)	1.28 (0.95–1.73)	0.11	
Recessive model[c]					
SNCA rs356219					
AA or AG	GG	1090 (49.9%)	1.00 (reference)	N/A	OR = 1.22
AA or AG	GA or AA	315 (14.4%)	0.72 (0.56–0.93)	0.011	95% CI = 0.78–1.92
GG	GG	623 (28.5%)	1.48 (1.21–1.83)	0.0002	*p* = 0.38
GG	GA or AA	156 (7.1%)	1.31 (0.93–1.87)	0.13	
SNCA rs11931074					
GG or GT	GG	1145 (50.6%)	1.00 (reference)	N/A	OR = 1.39
GG or GT	GA or AA	332 (14.7%)	0.66 (0.52–0.85)	0.0011	95% CI = 0.90–2.17
TT	GG	630 (27.8%)	1.38 (1.12–1.69)	0.0020	*p* = 0.14
TT	GA or AA	158 (7.0%)	1.27 (0.90–1.80)	0.18	

ORs and *p* values result from fixed-effects logistic regression models. For tests of association, the 2 given variants were combined into 1 variable, and the model was adjusted for site. For tests of interaction, models included each of the 2 variants, their interaction, and site. Additive models, genotype models, dominant models, and recessive models refer to the characterization of *SNCA* variants; only dominant models were considered for LRRK2 p.R1398H because of the small number of rare homozygotes for this variant. Key: CI, confidence interval; OR, odds ratio.

[a] Interaction ORs under an additive model are interpreted as the multiplicative increase in the effect of the minor allele for LRRK2 p.R1398H on PD corresponding to each additional risk allele for *SNCA* variants, or alternatively as the as the multiplicative increase in the effect of each additional risk allele for *SNCA* variants on PD corresponding to presence of the minor allele for LRRK2 p.R1398H.

[b] Interaction ORs under a dominant model are interpreted as the multiplicative increase in the effect of the minor allele for LRRK2 p.R1398H on PD corresponding to presence of the risk allele for *SNCA* variants, or alternatively as the as the multiplicative increase in the effect of presence of the risk allele for *SNCA* variants on PD corresponding to presence of the minor allele for LRRK2 p.R1398H.

[c] Interaction ORs under a recessive model are interpreted as the multiplicative increase in the effect of the minor allele for LRRK2 p.R1398H on PD corresponding to presence of 2 risk alleles for *SNCA* variants, or alternatively as the as the multiplicative increase in the effect of presence of 2 risk alleles for *SNCA* variants on PD corresponding to presence of the minor allele for LRRK2 p.R1398H.

[d] Tests of interaction under a genotype model do not produce a single interaction OR, and therefore only a *p* value is given.

subgroup of Asian individuals for whom that information was available (71%) and also under a random effects model (Supplementary Table 8). Interactions between LRRK2 p.R1398H and *SNCA* variants under additive and recessive models are shown in Supplementary Table 11 separately for each Asian country; between-site heterogeneity in interactions with *LRRK2* p.R1398H was moderate for both *SNCA* rs356219 and rs11931074 in the Asian series (I^2 = 46%–55%, $p \geq 0.084$, Supplementary Table 8).

4. Discussion

Recently, a 3-variant (p.N551K-R1398H-K1423K) haplotype in the *LRRK2* gene was shown to affect susceptibility to PD in a protective manner in both Caucasian and Asian populations (Ross et al., 2011; Tan et al., 2010). The p.R1398H substitution appears to be the most likely functional variant, as it is located in the conserved Roc domain, and there is supporting evidence of reduced kinase activity (Tan et al., 2010). Although a number of previous investigations have examined interactions between the well-validated PD susceptibility variants located in the *SNCA* and *MAPT* genes (Biernacka et al., 2011; Elbaz et al., 2011; Goris et al., 2007; Mamah et al., 2005; McCulloch et al., 2008; Simón-Sánchez et al., 2009; Trotta et al., 2012; Wider et al., 2011), no study reported to date has examined interactions of LRRK2 p.R1398H with *SNCA* and *MAPT* variants. The results of our large case-control study involving both Caucasian and Asian individuals indicate that the protective effect of LRRK2 p.R1398H is observed consistently for different *SNCA* and *MAPT* genotypes, whereas, similarly, the *SNCA* and *MAPT* risk effects are observed for individuals with and without the protective p.R1398H allele.

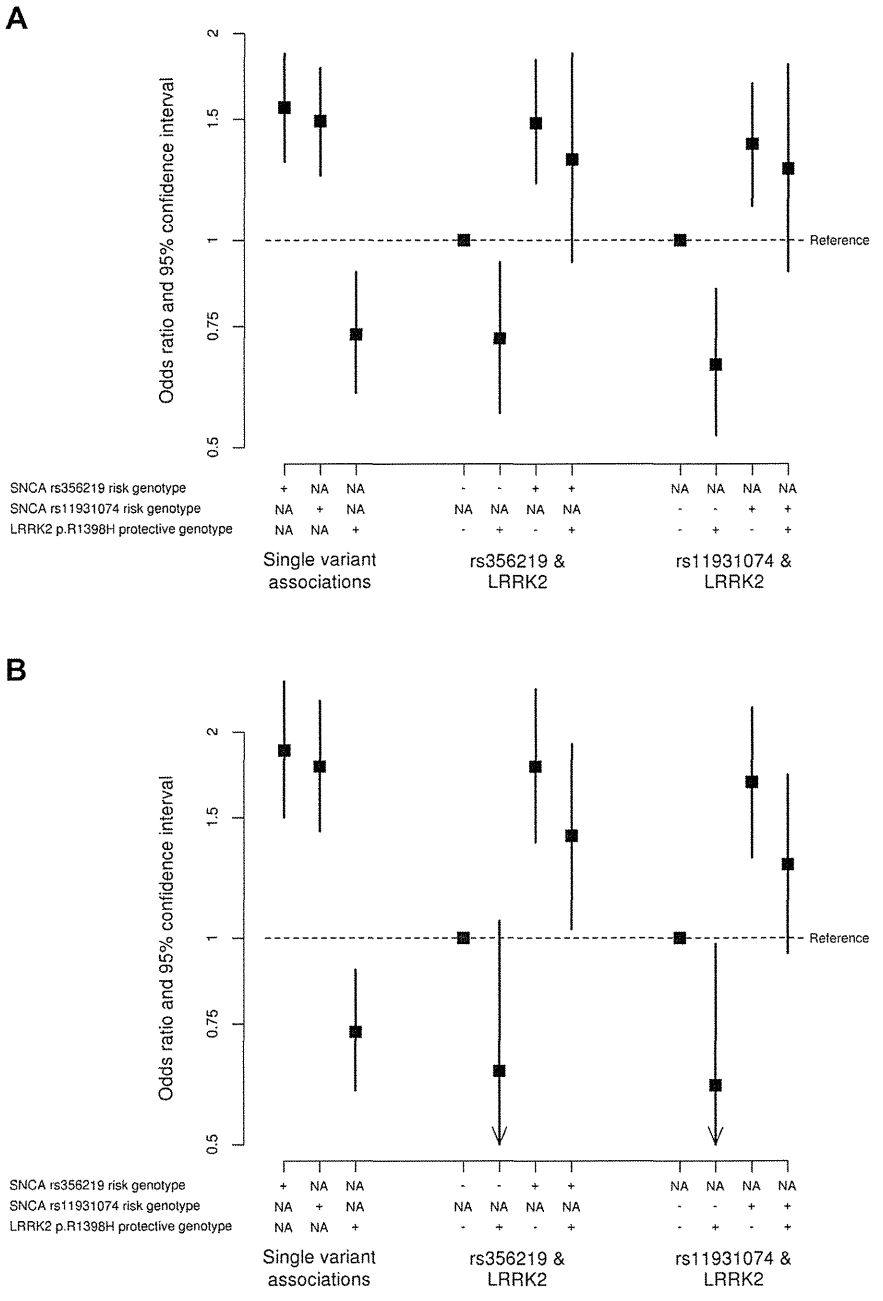

Fig. 2. (A) Individual and combined effects of *SNCA* rs356219, *SNCA* rs11931074, and LRRK2 p.R1398H on risk of Parkinson's disease (PD) in the Asian series. *SNCA* rs356219 and rs11931074 were considered under a recessive model (i.e., presence vs. absence of 2 copies of the minor allele). For *SNCA* rs356219, the risk genotype was GG. For *SNCA* rs11931074 , the risk genotype was TT. (B) Individual and combined effects of *SNCA* rs356219, *SNCA* rs11931074, and LRRK2 p.R1398H on risk of PD in the Asian series. *SNCA* rs356219 and rs11931074 were considered under a dominant model (i.e., presence vs. absence of the minor allele). For *SNCA* rs356219, the risk genotype was AG or GG. For *SNCA* rs11931074 , the risk genotype was GT or TT. (A and B) For LRRK2 p.R1398H, the protective genotype was GA or AA (i.e., presence of the minor allele). NA indicates that a given SNP was not involved in the particular portion of the analysis.

Despite the relatively large number of interactions and statistical models considered, the independent effects on PD risk for LRRK2 p.R1398H, *MAPT* rs1052553, and *SNCA* variants were observed with a very high level of consistency in our study. This was most apparent in the large Caucasian series, for which all interaction ORs were between 0.80 and 1.13, with the exception of the 2 aforementioned instances involving rare genotypes for *MAPT* rs1052553 and *SNCA* rs11931074. In addition, between-site heterogeneity in interaction effects was low to moderate in Caucasians. Although the protective effect of LRRK2 p.R1398H on risk of PD was observed consistently across *SNCA* variant genotypes in Asians, perhaps the least convincing evidence of lack of gene–gene interaction was observed in this series. Albeit not approaching significance even before adjustment for multiple testing, the magnitude of this observed protective effect was slightly smaller when the risk genotype for *SNCA* variants was present, whereas, conversely, the observed risk effects of *SNCA* variants were marginally stronger in individuals with the protective p.R1398H genotypes. In addition,

heterogeneity in interaction effects between sites was highest in the Asian series. However, it is important to highlight that it would be very unusual to observe a complete lack of gene–gene interaction (i.e., interaction OR = 1) in all scenarios simply because of natural sampling variability, particularly given the number of possible interactions that were examined. Nonetheless, given the smaller size of our Asian series in comparison to the Caucasian series, it will be important to validate our findings in larger series of Asian individuals.

Recent studies have supported our earlier work indicating that the effects of *SNCA* and *MAPT* variants on PD risk are independent of one another (Biernacka et al., 2011; Trotta et al., 2012; Wider et al., 2011). Although our current study is the first to date to examine the potential interaction of the protective LRRK2 p.R1398H substitution with *MAPT* and *SNCA* variants in regard to risk of PD, previous studies have evaluated interactions with, or combined effects of, *LRRK2* variants and those in *SNCA* and *MAPT*. In their analysis of 1098 patients with PD and 1098 matched controls from the United States (a subset of which were also used in the current study), Biernacka et al. (2011) found no statistically significant evidence of gene–gene interaction when considering 8 intronic *LRRK2* variants, 10 *SNCA* variants (8 intronic, 1 3′ downstream and 1 5′ Rep1), and 8 *MAPT* variants (6 intronic, 1 3′ UTR, and 1 H1/H2). Wang et al. (2012) concluded that other genes, including *MAPT* and *SNCA*, modified *LRRK2*-related risk for PD in a Chinese cohort of 2013 sporadic PD patients and 1971 controls. This was based on findings that, in comparison to individuals harboring only the LRRK2 p.G2385R or p.R1628P risk variants, the risk of PD is increased in individuals with these and other PD risk variants. However, it is unclear whether this represents independent or interactive effects, and the sample sizes of the combined risk-variant groups examined were quite small. The results of these studies are consistent with those of our own, with the effect of *LRRK2* variants on PD susceptibility appearing to be independent of *SNCA* and *MAPT* risk factors for PD.

The strengths of our study, including the large sample size and inclusion of subjects from a variety of different populations, are important to highlight; however, several limitations should also be acknowledged. A key question is whether the lack of interaction of LRRK2 p.R1398H with *SNCA* and *MAPT* variants is a consequence of sample size or the frequencies of the examined variants. To assess the possibility of a false-negative association, it is most helpful to examine 95% confidence limits for observed interaction odds ratio estimates (Goodman and Berlin, 1994). These confidence limits were generally relatively tight in the larger Caucasian series, indicating a lack of a biologically significant interaction in this population, but were wider in the Asian series, further highlighting the need for validation of our findings in that series. In addition, as is generally the case for large-scale collaborative studies attempting to address a focused research question that involves a small number of genetic variants, without available genome-wide population control markers, population stratification could potentially have had an impact on our results. However, this potential limitation is lessened by the fact that our logistic regression models were adjusted by site, which makes any possible population stratification a site-specific issue. Other limitations of our study include the different diagnostic criteria across the different sites and the lack of a standardized inclusion/exclusion criteria for patients with PD and controls.

In conclusion, our study provides evidence that the effect of LRRK2 p.R1398H on risk of PD is independent of the *MAPT* H1-haplotype defining variant rs1052553 and *SNCA* variants, and vice versa. This lack of gene–gene interaction was apparent in both our large Caucasian patient-control series and our smaller Asian series. Evaluation of interactions involving individuals of other ethnic backgrounds, other rarer *LRRK2* susceptibility variants, and PD susceptibility variants at other loci (Lill et al., 2012) is needed in order to move toward a fuller understanding of the genetic architecture of PD susceptibility.

Disclosure statement

J.O.A., M.J.F., and Z.K.W. report holding a patent on *LRRK2* genetic variability. M.J.F. has received royalties for licensing of genetically modified *LRRK2* mouse models. D.M.M. declares a patent pending entitled "Methods to Treat PD." C.K. and R.K. declare receiving payment in their role as consultants for Centogene and Takeda Pharmaceutical, respectively. All other authors declare that they have no conflicts of interest.

Acknowledgements

This work was supported by a grant from The Michael J. Fox Foundation for Parkinson's Research (O.A.R., M.J.F.). Original funding for the GEO-PD was supported by a grant from The Michael J. Fox Foundation for Parkinson's Research Edmond J. Safra Global Genetics Consortia program (D.M.M.). The Mayo Clinic Jacksonville is a Morris K. Udall Center of Excellence in Parkinson's Disease Research (grant no. P50 NS072187) and was supported by a the gift from the family of Carl Edward Bolch, Jr, and Susan Bass Bolch (R.J.U., Z.K.W., O.A.R.). O.A.R. acknowledges funding support from the National Institutes of Health (grant no. R01 NS078086). This research was undertaken, in part, thanks to funding from the Canada Excellence Research Chairs program (M.J.F., C.V.G.). Leading Edge Endowment Funds, provided by the Province of British Columbia, LifeLabs, and Genome BC, support the Dr Donald Rix BC Leadership Chair (M.J.F.). D.M.M. acknowledges the National Institutes of Health for funding support (grant no. R01ES10751). Studies at individual sites were supported by a number of different funding agencies world-wide including; Italian Ministry of Health (Ricerca Corrente, Ricerca Finalizzata); the Swedish Parkinson Academy; the Swedish Parkinson Foundation; the Federal Ministry for Education and Research (BMBF, NGFNplus; 01GS08134) (R.K.); the NGFNplus (Neuron-Parkinson-subproject 7) (S.G.); CHRU de Lille, University of Lille 2, INSERM; French Ministry PHRCs (1994/, 2002/1918, 2005/1914); Association France Parkinson (2005); Fondation de France 2004-013306; Fondation de la Recherche Médicale (2006); PPF (synucléothèque 2005–2009); the 2 Centres de Ressources Biologiques (IPL-Lille, CHRU-Lille) and its scientific committee (A.D., M.C.C.H., Philippe Amouyel, Florence Pasquier, Régis Bordet); funding from France-Parkinson Association and the program "Investissement d'avenir" ANR-10-IAIHU-06; the Swedish Research Council; the Swedish Society for Medical Research; the Swedish Society of Medicine; funds from the Karolinska Institutet and the Parkinson Foundation in Sweden (K.W.); the National Institutes of Health and National Institute of Neurological Disorders and Stroke (grant nos. 1RC2NS070276, NS057567, and P50NS072187); Mayo Clinic Florida Research Committee CR programs (M.J.F., Z.K.W.); the Geriatric Medical Foundation of Queensland (G.D.M.); a career development award from the Volkswagen Foundation and from the Hermann and Lilly Schilling Foundation (C.K.); the Research Committee of University of Thessaly (code 2845); and Laboratory of Neurogenetics, Biomedicine Department, CERETETH, Larissa, Greece (code 01-04-207) (G.H., E.D.).

A number of individuals must be acknowledged for their contributions to make this work possible; Ferdinanda Annesi, PhD; Patrizia Tarantino, PhD (Institute of Neurological Sciences, National Research Council); Monica Gagliardi, PhD, (Institute of Neurological Sciences, National Research Council, Cosenza Italy), Chiara Riva,

PhD (Department of Neuroscience and Biomedical Technologies, University of Milano-Bicocca, Monza, Italy); Roberto Piolti, MD (Department of Neurology, Ospedale San Gerardo, Monza, Italy); Alessandro Ferraris MD, PhD (IRCCS Casa Sollievo della Sofferenza Hospital, Mendel Laboratory, San Giovanni Rotondo, Italy); Aurélie Duflot, (UMR837 Inserm-Univ Lille 2, CHRU de Lille), Jean-Philippe Legendre, Nawal Waucquier (Neurologie et Pathologie du Mouvement, Clinique de Neurologie du CHU de Lille). Anna Rita Bentivoglio, MD, PhD, Tamara Ialongo, MD, PhD, Arianna Guidubaldi, MD, Carla Piano, MD (Institute of Neurology, Catholic University, Rome, Italy); Phil Hyu Lee, MD, PhD (Department of Neurology, Yonsei University College of Medicine, Seoul, Korea); Jan Reimer (Department of Neurology, Skåne University Hospital, Sweden); Hiroyo Yoshino, PhD, Manabu Funayama, PhD, Yuanzhe Li, MD, PhD (Juntendo University School of Medicine, Tokyo, Japan). From the Queensland Parkinson's Project: R.S. Boyle and A. Sellbach (Princess Alexandra Hospital, Brisbane), J. D. O'Sullivan (Royal Brisbane and Women's Hospital, Brisbane), G.T. Sutherland, G.A. Siebert and N.N.W. Dissanayaka (Eskitis Institute for Cell and Molecular Therapies, Griffith University, Nathan, QLD).

Finally, we acknowledge all of the patients and control subjects who kindly donated DNA to make collaborative studies like these possible.

A full list of GEO-PD consortium member sites is provided in the Supplementary Text.

Appendix A. Supplementary data

Supplementary data associated with this article can be found, in the online version, at http://dx.doi.org/10.1016/j.neurobiolaging.2013.07.013.

References

Biernacka, J.M., Armasu, S.M., Cunningham, J.M., Ahlskog, J.E., Chung, S.J., Maraganore, D.M., 2011. Do interactions between SNCA, MAPT, and LRRK2 genes contribute to Parkinson's disease susceptibility? Parkinsonism Relat. Disord. 17, 730–736.

Bower, J.H., Maraganore, D.M., McDonnell, S.K., Rocca, W.A., 1999. Incidence and distribution of parkinsonism in Olmstead County, Minnesota, 1976-1990. Neurology 52, 1214–1220.

Chen, L., Zhang, S., Liu, Y., Hong, H., Wang, H., Zheng, Y., Zhou, H., Chen, J., Xian, W., He, Y., Li, J., Liu, Z., Pei, Z., Zeng, J., 2011. LRRK2 R1398H polymorphism is associated with decreased risk of Parkinson's disease in a Han Chinese population. Parkinsonism Relat. Disord. 17, 291–292.

de Lau, L.M., Breteler, M.M., 2006. Epidemiology of Parkinson's disease. Lancet Neurol. 5, 525–535.

DerSimonian, R., Laird, N., 1986. Meta-analysis in clinical trials. Control Clin. Trials 7, 177–188.

Di Fonzo, A., Wu-Chou, Y.H., Lu, C.S., van Doeselaar, M., Simons, E.J., Rohé, C.F., Chang, H.C., Chen, R.S., Weng, Y.H., Vanacore, N., Breedveld, G.J., Oostra, B.A., Bonifati, V., 2006. A common missense variant in the LRRK2 gene, Gly2385Arg, associated with Parkinson's disease risk in Taiwan. Neurogenetics 7, 133–138.

Elbaz, A., Ross, O.A., Ioannidis, J.P., Soto-Ortolaza, A.I., Moisan, F., Aasly, J., Annesi, G., Bozi, M., Brighina, L., Chartier-Harlin, M.C., Destée, A., Ferrarese, C., Ferraris, A., Gibson, J.M., Gispert, S., Hadjigeorgiou, G.M., Jasinska-Myga, B., Klein, C., Krüger, R., Lambert, J.C., Lohmnan, K., van de Loo, S., Loriot, M.A., Lynch, T., Mellick, G.D., Mutez, E., Nilsson, C., Opala, G., Puschmann, A., Quattrone, A., Sharma, M., Silburn, P.A., Stefanis, L., Uitti, R.J., Valente, E.M., Vilariño-Güell, C., Wirdefeldt, K., Wszolek, Z.K., Xiromerisiou, G., Maraganore, D.M., Farrer, M.J.; Genetic Epidemiology of Parkinson's Disease (GEO-PD) Consortium, 2011. Independent and joint effects of the MAPT and SNCA genes in Parkinson disease. Ann. Neurol. 69, 778–792.

Evans, W., Fung, H.C., Steele, J., Eerola, J., Tienari, P., Pittman, A., Silva, R.d., Myers, A., Vrieze, F.W., Singleton, A., Hardy, J., 2004. The tau H2 haplotype is almost exclusively Caucasian in origin. Neurosci. Lett. 369, 183–185.

Farrer, M.J., Stone, J.T., Lin, C.H., Dächsel, J.C., Hulihan, M.M., Haugarvoll, K., Ross, O.A., Wu, R.M., 2007. Lrrk2 G2385R is an ancestral risk factor for Parkinson's disease in Asia. Parkinsonism Relat. Disord. 13, 89–92.

Gasser, T., Hardy, J., Mizuno, Y., 2011. Milestones in PD genetics. Mov. Disord. 26, 1042–1048.

Gelb, D.J., Oliver, E., Gilman, S., 1999. Diagnostic criteria for Parkinson disease. Arch. Neurol. 56, 33–39.

Goodman, S.N., Berlin, J.A., 1994. The use of predicted confidence intervals when planning experiments and the misuse of power when interpreting results. Ann. Intern. Med. 121, 200–206.

Goris, A., Williams-Gray, C.H., Clark, G.R., Foltynie, T., Lewis, S.J., Brown, J., Ban, M., Spillantini, M.G., Compston, A., Burn, D.J., Chinnery, P.F., Barker, R.A., Sawcer, S.J., 2007. Tau and alpha-synuclein in susceptibility to, and dementia in, Parkinson's disease. Ann. Neurol. 62, 145–153.

Healy, D.G., Abou-Sleiman, P.M., Lees, A.J., Casas, J.P., Quinn, N., Bhatia, K., Hingorani, A.D., Wood, N.W., 2004. Tau gene and Parkinson's disease: a case-control study and meta-analysis. J. Neurol. Neurosurg. Psychiatry 75, 962–965.

Heckman, M.G., Soto-Ortolaza, A.I., Aasly, J.O., Abahuni, N., Annesi, G., Bacon, J.A., Bardien, S., Bozi, M., Brice, A., Brighina, L., Carr, J., Chartier-Harlin, M.C., Dardiotis, E., Dickson, D.W., Diehl, N.N., Elbaz, A., Ferrarese, C., Fiske, B., Gibson, J.M., Gibson, R., Hadjigeorgiou, G.M., Hattori, N., Ioannidis, J.P., Boczarska-Jedynak, M., Jasinska-Myga, B., Jeon, B.S., Kim, Y.J., Klein, C., Kruger, R., Kyratzi, E., Lesage, S., Lin, C.H., Lynch, T., Maraganore, D.M., Mellick, G.D., Mutez, E., Nilsson, C., Opala, G., Park, S.S., Petrucci, S., Puschmann, A., Quattrone, A., Sharma, M., Silburn, P.A., Sohn, Y.H., Stefanis, L., Tadic, V., Theuns, J., Tomiyama, H., Uitti, R.J., Valente, E.M., Van Broeckhoven, C., van de Loo, S., Vassilatis, D.K., Vilariño-Güell, C., White, L.R., Wirdefeldt, K., Wszolek, Z.K., Wu, R.M., Hentati, F., Farrer M.J., Ross OA; on behalf of the Genetic Epidemiology of Parkinson's Disease (GEO-PD) Consortium., Population-specific frequencies for LRRK2 susceptibility variants in the genetic epidemiology of Parkinson's disease (GEO-PD) consortium. Mov. Disord. In press.

Higgins, J.P., Thompson, S.G., 2002. Quantifying heterogeneity in a meta-analysis. Stat. Med. 21, 1539–1558.

Hughes, A.J., Daniel, S.E., Kilford, L., Lees, A.J., 1992. Accuracy of clinical diagnosis of idiopathic Parkinson's disease: a clinic-pathological study of 100 cases. J. Neurol. Neurosurg. Psychiatry 55, 181–184.

Nalls, M.A., Plagnov, V., Hernandez, D.G., Sharma, M., Sheerin, U.M., Saad, M., Simón-Sánchez, J., Schulte, C., Lesage, S., Sveinbjörnsdóttir, S., Stefánsson, K., Martinez, M., Hardy, J., Heutink, P., Brice, A., Gasser, T., Singleton, A.B., Wood, N.W., International Parkinson Disease Genomics Consortium, 2011. Imputation of sequence variants for identification of genetic risks for Parkinson's disease: a meta-analysis of genome-wide association studies. Lancet 377, 641–649.

Krüger, R., Vieira-Saecker, A.M., Kuhn, W., Berg, D., Müller, T., Kühnl, N., Fichs, G.A., Storch, A., Hungs, M., Woitalla, D., Przuntek, H., Epplen, J.T., Schöls, L., Riess, O., 1999. Increased susceptibility to sporadic Parkinson's disease by a certain combined alpha-synuclein/apolipoprotein E genotype. Ann. Neurol. 45, 611–617.

Lill, C.M., Roehr, J.T., McQueen, M.B., Kavvoura, F.K., Bagade, S., Schjeide, B.M., Schjeide, L.M., Meissner, E., Zauft, U., Allen, N.C., Liu, T., Schilling, M., Anderson, K.J., Beecham, G., Berg, D., Biernacka, J.M., Brice, A., DeStefano, A.L., Do, C.B., Eriksson, N., Factor, S.A., Farrer, M.J., Foroud, T., Gasser, T., Hamza, T., Hardy, J.A., Heutink, P., Hill-Burns, E.M., Klein, C., Latourelle, J.C., Maraganore, D.M., Martin, E.R., Martinez, M., Myers, R.H., Nalls, M.A., Pankratz, N., Payami, H., Satake, W., Scott, W.K., Sharma, M., Singleton, A.B., Stefansson, K., Toda, T., Tung, J.Y., Vance, J., Wood, N.W., Zabetian, C.P., Young, P., Tanzi, R.E., Khoury, M.J., Zipp, F., Lehrach, H., Ioannidis, J.P., Bertram, L.; 23andMe Genetic Epidemiology of Parkinson's Disease Consortium; International Parkinson's Disease Genomics Consortium; Parkinson's Disease GWAS Consortium; Welcome Trust Case Control Consortium 2 (WTCCC2), 2012. Comprehensive research synopsis and systemic meta-analyses in Parkinson's disease genetics: the PDGene database. PLoS Genet. 8, e10002548.

Mamah, C.E., Lesnick, T.G., Lincoln, S.J., Strain, K.J., de Andrade, M., Bower, J.H., Ahlskog, J.E., Rocca, W.A., Farrer, M.J., Maraganore, D.M., 2005. Interaction of alpha-synuclein and tau genotypes in Parkinson's disease. Ann. Neurol. 57, 439–443.

Maraganore, D.M., de Andrade, M., Elbaz, A., Farrer, M.J., Ioannidis, J.P., Krüger, R., Rocca, W.A., Schneider, N.K., Lesnick, T.G., Lincoln, S.J., Hulihan, M.M., Aasly, J.O., Ashizawa, T., Chartier-Harlin, M.C., Checkoway, H., Ferrarese, C., Hadjigeorgiou, G., Hattori, N., Kawakami, H., Lambert, J.C., Lynch, T., Mellick, G.D., Papapetropoulus, S., Parsian, A., Quattrone, A., Riess, O., Tan, E.K., Van Broeckhoven, C., Genetic Epidemiology of Parkinson's Disease (GEO-PD) Consortium, 2006. Collaborative analysis of alpha-synuclein gene promoter variability in Parkinson disease. JAMA 296, 661–670.

McCulloch, C.C., Kay, D.M., Factor, S.A., Samii, A., Nutt, J.G., Higgins, D.S., Griffith, A., Roberts, J.W., Leis, B.C., Montimurro, J.S., Zabetian, C.P., Payami, H., 2008. Exploring gene-environment interactions in Parkinson's disease. Hum. Genet. 123, 257–265.

Mizuta, I., Satake, W., Nakabayashi, Y., Ito, C., Suzuki, S., Momose, Y., Nagai, Y., Oka, A., Inoko, H., Fukae, J., Saito, Y., Sawabe, M., Murayama, S., Yamamoto, M., Hattori, N., Murata, M., Toda, T., 2006. Multiple candidate gene analysis identifies alpha-synuclein as a susceptibility gene for sporadic Parkinson's disease. Hum. Mol. Genet. 15, 1151–1158.

Mueller, J.C., Fuchs, J., Hofer, A., Zimprich, A., Lichtner, P., Illig, T., Berg, D., Wüllner, U., Meitinger, T., Gasser, T., 2005. Multiple regions of alpha-synuclein are associated with Parkinson's disease. Ann. Neurol. 57, 535–541.

Pankratz, N., Wilk, J.B., Latourelle, J.C., DeStefano, A.L., Halter, C., Pugh, E.W., Doheny, K.F., Gusella, J.F., Nichols, W.C., Foroud, T., Myers, R.H., PSG-PROGENI and GenePD Investigators, Coordinators and Molecular Genetic Laboratories, 2009. Genomewide association study for susceptibility genes contributing to familial Parkinson disease. Hum. Genet. 124, 593–605.

Postuma, R.B., Montplaisir, J., 2009. Predicting Parkinson's disease—why, when, and how? Parkinsonism Relat. Disord. 15(suppl 3), S105–S109.

Ross, O.A., Gosal, D., Stone, J.T., Lincoln, S.J., Heckman, M.G., Irvine, G.B., Johnston, J.A., Gibson, J.M., Farrer, M.J., Lynch, T., 2007. Familial genes in sporadic disease: common variants of alpha-synuclein gene associate with Parkinson's disease. Mech. Aging Dev. 128, 378–382.

Ross, O.A., Wu, Y.R., Lee, M.C., Funayama, M., Chen, M.L., Soto, A.I., Mata, I.F., Lee-Chen, G.J., Chen, C.M., Tang, M., Zhao, Y., Hattori, N., Farrer, M.J., Tan, E.K., Wu, R.M., 2008. Analysis of Lrrk2 R1628P as a risk factor for Parkinson's disease. Ann. Neurol. 64, 88–92.

Ross, O.A., Soto-Ortolaza, A.I., Heckman, M.G., Aasly, J.O., Abahuni, N., Annesi, G., Bacon, J.A., Bardien, S., Bozi, M., Brice, A., Brighina, L., Van Broeckhoven, C., Carr, J., Chartier-Harlin, M.C., Dardiotis, E., Dickson, D.W., Diehl, N.N., Elbaz, A., Ferrarese, C., Ferraris, A., Fiske, B., Gibson, J.M., Gibson, R., Hadjigeorgiou, G.M., Hattori, N., Ioannidis, J.P., Jasinska-Myga, B., Jeon, B.S., Kim, Y.J., Klein, C., Kruger, R., Kyratzi, E., Lesage, S., Lin, C.H., Lynch, T., Maraganore, D.M., Mellick, G.D., Mutez, E., Nilsson, C., Opala, G., Park, S.S., Puschmann, A., Quattrone, A., Sharma, M., Silburn, P.A., Sohn, Y.H., Stefanis, L., Tadic, V., Theuns, J., Tomiyama, H., Uitti, R.J., Valente, E.M., van de Loo, S., Vassilatis, D.K., Vilariño-Güell, C., White, L.R., Wirdefeldt, K., Wszolek, Z.K., Wu, R.M., Farrer, M.J.; Genetic Epidemiology of Parkinson's Disease (GEO-PD) Consortium, 2011. Association of LRRK2 exonic variants with susceptibility to Parkinson's disease: a case control study. Lancet Neurol. 10, 898–908.

Satake, W., Nakabayashi, Y., Mizuta, I., Hirota, Y., Ito, C., Kubo, M., Kawaguchi, T., Tsunoda, T., Watanabe, M., Takeda, A., Tomiyama, H., Nakashima, K., Hasegawa, K., Obata, F., Yoshikawa, T., Kawakami, H., Sakoda, S., Yamamoto, M., Hattori, N., Murata, M., Nakamura, Y., Toda, T., 2009. Genome-wide association study identifies common variants at four loci as genetic risk factors for Parkinson's disease. Nat. Genet. 41, 1303–1307.

Simón-Sánchez, J., Schulte, C., Bras, J.M., Sharma, M., Gibbs, J.R., Berg, D., Paisan-Ruiz, C., Lichtner, P., Scholz, S.W., Hernandez, D.G., Krüger, R., Federoff, M., Klein, C., Goate, A., Perlmutter, J., Bonin, M., Nalls, M.A., Illig, T., Gieger, C., Houlden, H., Steffens, M., Okun, M.S., Racette, B.A., Cookson, M.R., Foote, K.D., Fernandez, H.H., Traynor, B.J., Schreiber, S., Arepalli, S., Zonozi, R., Gwinn, K., van der Brug, M., Lopez, G., Chancock, S.J., Schatzkin, A., Park, Y., Hollenbeck, A., Gao, J., Huang, X., Wood, N.W., Lorenz, D., Deuschl, G., Chen, H., Riess, O., Hardy, J.A., Singleton, A.B., Gasser, T., 2009. Genome-wide association study reveals genetic risk underlying Parkinson's disease. Nat. Genet. 41, 1308–1312.

Skipper, L., Wilkes, K., Toft, M., Baker, M., Lincoln, S., Hulihan, M., Ross, O.A., Hutton, M., Aasly, J., Farrer, M.J., 2004. Linkage disequilibrium and association of MAPT H1 in Parkinson disease. Am. J. Hum. Genet. 75, 669–677.

Tan, E.K., Peng, R., Teo, Y.Y., Tan, L.C., Angeles, D., Ho, P., Chen, M.L., Lin, C.H., Mao, X.Y., Chang, X.L., Prakash, K.M., Liu, J.J., Au, W.L., Le, W.D., Jankovic, J., Burgunder, J.M., Zhao, Y., Wu, R.M., 2010. Multiple LRRK2 variants modulate risk of Parkinson disease: a Chinese multicenter study. Hum. Mutat. 31, 561–568.

Tobin, J.E., Latourelle, J.C., Lew, M.F., Klein, C., Suchowersky, O., Shill, H.A., Golbe, L.I., Mark, M.H., Growdon, J.H., Wooten, G.F., Racette, B.A., Perlmutter, J.S., Watts, R., Guttman, M., Baker, K.B., Goldwurm, S., Pezzoli, G., Singer, C., Saint-Hilaire, M.H., Hendricks, A.E., Williamson, S., Nagle, M.W., Wilk, J.B., Massood, T., Laramie, J.M., DeStefano, A.L., Litvan, I., Nicholson, G., Corbett, A., Isaacson, S., Burn, D.J., Chinnery, P.F., Pramstaller, P.P., Sherman, S., Al-hinti, J., Drasby, E., Nance, M., Moller, A.T., Ostergaard, K., Roxburgh, R., Snow, B., Slevin, J.T., Cambi, F., Gusella, J.F., Myers, R.H., 2008. Haplotypes and gene expression implicate the MAPT region for Parkinson disease: the GenePD Study. Neurology 71, 28–34.

Trotta, L., Guella, I., Soldà, G., Sironi, F., Tesei, S., Canesi, M., Pezzoli, G., Goldwurn, S., Duga, S., Asselta, R., 2012. SNCA and MAPT genes: independent and joint effects in Parkinson disease in the Italian population. Parkinsonism Relat. Disord. 18, 257–262.

Wang, C., Cai, Y., Zheng, Z., Tang, B.S., Xu, Y., Wang, T., Ma, J., Chen, S.D., Langston, J.W., Tanner, C.M., Chan, P.; Chinese Parkinson Study Group (CPSG), 2012. Penetrance of LRRK2 G2385R and R1628P is modified by common PD-associated genetic variants. Parkinsonism Relat. Disord. 18, 958–963.

Weinberg, C.R., 1986. Applicability of the simple independent action model to epidemiologic studies involving two factors and a dichotomous outcome. Am. J. Epidemiol. 123, 162–173.

Wider, C., Vilariño-Güell, C., Jasinska-Myga, B., Heckman, M.G., Soto-Ortolaza, A.I., Cobb, S.A., Aasly, J.O., Gibson, J.M., Lynch, T., Uitti, R.J., Wszolek, Z.K., Farrer, M.J., Ross, O.A., 2010. Association of the MAPT locus with Parkinson's disease. Eur. J. Neurol. 17, 483–486.

Wider, C., Vilariño-Güell, C., Heckman, M.G., Jasinska-Myga, B., Ortolaza-Soto, A.I., Diehl, N.N., Crook, J.E., Cobb, S.A., Bacon, J.A., Aasly, J.O., Gibson, J.M., Lynch, T., Uitti, R.J., Wszolek, Z.K., Farrer, M.J., Ross, O.A., 2011. SNCA, MAPT, and GSK3B in Parkinson disease: a gene-gene interaction study. Eur. J. Neurol. 18, 876–881.

Winkler, S., Hagenah, J., Lincoln, S., Heckman, M., Haugarvoll, K., Lohmann-Hedrich, K., Kostic, V., Farrer, M., Klein, C., 2007. alpha-Synuclein and Parkinson disease susceptibility. Neurology 69, 1745–1750.

nature COMMUNICATIONS

ARTICLE

Received 9 Sep 2013 | Accepted 11 Apr 2014 | Published 29 May 2014

DOI: 10.1038/ncomms4932 OPEN

TRPV2 is critical for the maintenance of cardiac structure and function in mice

Yuki Katanosaka[1], Keiichiro Iwasaki[1], Yoshihiro Ujihara[1,2], Satomi Takatsu[1], Koki Nishitsuji[1], Motoi Kanagawa[3], Atsushi Sudo[3], Tatsushi Toda[3], Kimiaki Katanosaka[4,5], Satoshi Mohri[1,2] & Keiji Naruse[1,6]

The heart has a dynamic compensatory mechanism for haemodynamic stress. However, the molecular details of how mechanical forces are transduced in the heart are unclear. Here we show that the transient receptor potential, vanilloid family type 2 (TRPV2) cation channel is critical for the maintenance of cardiac structure and function. Within 4 days of eliminating TRPV2 from hearts of the adult mice, cardiac function declines severely, with disorganization of the intercalated discs that support mechanical coupling with neighbouring myocytes and myocardial conduction defects. After 9 days, cell shortening and Ca^{2+} handling by single myocytes are impaired in TRPV2-deficient hearts. TRPV2-deficient neonatal cardiomyocytes form no intercalated discs and show no extracellular Ca^{2+}-dependent intracellular Ca^{2+} increase and insulin-like growth factor (IGF-1) secretion in response to stretch stimulation. We further demonstrate that IGF-1 receptor/PI3K/Akt pathway signalling is significantly downregulated in TRPV2-deficient hearts, and that IGF-1 administration partially prevents chamber dilation and impairment in cardiac pump function in these hearts. Our results improve our understanding of the molecular processes underlying the maintenance of cardiac structure and function.

[1] Department of Cardiovascular Physiology, Graduate School of Medicine, Dentistry and Pharmaceutical Sciences, Okayama University, Shikata-cho 2-5-1, Okayama city, Okayama 700-8558, Japan. [2] Department of Physiology, Kawasaki Medical School, Matsushima 577, Kurashiki, Okayama 701-0192, Japan. [3] Division of Neurology/Molecular Brain Science, Kobe University Graduate School of Medicine, Kobe 650-0017, Japan. [4] Department of Neuroscience II, Research Institute of Environmental Medicine, Nagoya University, Furo-cho, Chikusa-ku, Nagoya, Aichi 464-8601, Japan. [5] College of Life and Health Sciences, Chubu University, Matsumoto-cho 1200, Kasugai, Aichi 487-8501, Japan. [6] ICORP-SORST-Cell Mechanosensing Project, Japan Science and Technology Agency, Nagoya, Aichi 466-8550, Japan. Correspondence and requests for materials should be addressed to Y.K. (email: ytanigu@md.okayama-u.ac.jp).

Mechanical forces provide essential physiological information for homeostatic regulation and functional adaptation at the levels of cells and organs[1]. In cardiovascular systems, cellular mechanical responses to haemodynamic stress are crucial for normal cardiac function, and affect both the physiological and the pathological growth of the heart[2,3]. More specifically, an increased cardiac workload resulting from exercise, pregnancy or postnatal growth promotes the physiological growth of the heart, whereas chronic hypertension can cause pathological hypertrophy[3]. Atrophy of the heart is a complication of protracted bed rest, prolonged weightlessness during space travel, and mechanical unloading with a ventricular assist device[3]. Despite the obvious influence of mechanical load on cardiac structure and function, the molecular details of the myocardial mechanotransduction required to maintain cardiac structure and function have remained unclear.

The heart is a functional syncytium composed of terminally differentiated myocytes specialized for excitation–contraction (E–C) coupling[3]. Individual cardiomyocytes are electrically and mechanically coupled at their termini, where highly organized cell–cell junctions known as intercalated discs are located[4–6]. The structure of intercalated discs is known to be remodelled in response to haemodynamic stress[7]. High wall stress increases the myocardial contractile force exerted as a result of cardiac hypertrophy, and the intercalated disc structure has to be optimized for physical robustness to adapt to this force[3]. By contrast, mechanical unloading causes cardiac atrophy, accompanied by disorder in the intercalated disc structure[7–10]. In addition, human cardiomyopathies have been associated with mutations in genes encoding components of intercalated discs, involved in mechanical coupling, and studies in mice and humans have suggested a connection between faulty myocardial mechanical coupling mechanisms and heart disease[11–15]. Flexibility in cardiac adaptation to haemodynamic stress probably requires the maintenance of intercalated disc structure and function by continuous monitoring of the mechanical stress at intercalated discs. Therefore, we hypothesized that cardiac mechanoreceptors at intercalated discs detect mechanical stress in the heart, maintaining myocardial structure and function in response to haemodynamic stress through the mechanical feedback system in cardiomyocytes.

Members of the transient receptor potential (TRP) cation channel family are potential candidates for the mechanoreceptors responding to tension, flow or changes in cell volume[16]. Previously, we reported that recombinant TRP, vanilloid family type 2 (TRPV2) can be activated by hypotonicity- and stretch-induced mechanical stimulation in ectopic expression systems[17,18]. Interestingly, TRPV2 is highly localized to mammalian cardiac intercalated discs, and its increased expression at the sarcolemma is observed in dystrophic human patients and animal models deficient in dystrophin or δ-sarcoglycan[17]. To elucidate the physiological role of cardiac TRPV2, we generated temporally controlled cardiac-specific TRPV2-deficient mice. Cardiac-specific TRPV2 elimination led to a severe decline in the heart's pump function with the disorganization of the intercalated disc structure, conduction defects and accelerated mortality. TRPV2-deficient neonatal cardiomyocytes formed no intercalated discs and showed no extracellular Ca^{2+}-dependent intracellular Ca^{2+} increase and IGF-1 secretion after stretch stimulation. TRPV2-deficient hearts showed downregulation of IGF-1 receptor/PI3K/Akt signalling. In addition, IGF-1 administration partially prevented chamber dilation and improved cardiac pump function in TRPV2-deficient hearts. These results suggest an indispensable role for TRPV2 in the maintenance of cardiac structure and function.

Results

Generation of cardiac-specific TRPV2-deficient mice. Initially, mice carrying a $TRPV2^{flox/flox}$ allele were generated by flanking exon 4 of the *TRPV2* gene with two *loxP* sequences (Supplementary Fig. 1). Excision of this segment resulted in a frameshift mutation downstream of the deletion sites. Translation from the first ATG gave rise to a short, 92 amino-acid (aa) product containing 62 aa of the original TRPV2 protein; however, most of the TRPV2 channel structure was lost after *Cre*-mediated recombination. We crossed mice bearing the $TRPV2^{flox/flox}$ allele with a transgenic line (*MerCreMer*) expressing *Cre* recombinase under the control of the α-myosin heavy chain promoter in a tamoxifen-inducible cardiomyocyte-specific manner[19] to produce $TRPV2^{flox/flox}$;$MerCreMer^{+/-}$ mice. To account for the deleterious effect of potential nonspecific *Cre* recombinase-mediated cardiotoxicity[20], we used $TRPV2^{flox/+}$; $MerCreMer^{+/-}$ and $TRPV2^{flox/flox}$;$MerCreMer^{-/-}$ littermates as age-matched controls, from which $TRPV2^{flox/flox}$; $MerCreMer^{+/-}$ mice were indistinguishable in appearance. The $TRPV2^{flox/flox}$;$MerCreMer^{+/-}$ mice were genotyped by PCR using primers for *Cre-loxP* sites and *Cre* recombinase (Fig. 1a and Supplementary Fig. 1). In adult $TRPV2^{flox/flox}$; $MerCreMer^{+/-}$ mice treated with tamoxifen for 3 days (daily dose of 8 mg kg^{-1}), we confirmed successful *Cre* recombination by PCR amplification of cardiac genomic DNA, to detect the deleted allele (Fig. 1b). Consistently, the expression of TRPV2 messenger RNA was dramatically suppressed in the hearts of TRPV2-deficient mice on day 3 (Fig. 1c). There was an ~95% reduction in TRPV2 protein in membrane extracts of cardiac muscle from these mice after 4 days of tamoxifen treatment (Fig. 1d). Consistently, the TRPV2 protein was also not detectable by immunofluorescent staining at intercalated discs in the hearts of these mice, although TRPV2 was highly localized to intercalated discs in control mice (Fig. 1e). Hereafter, in this study, we treated $TRPV2^{flox/flox}$;$MerCreMer^{+/-}$, $TRPV2^{flox/+}$; $MerCreMer^{+/-}$ and $TRPV2^{flox/flox}$;$MerCreMer^{-/-}$ mice with 8 mg kg^{-1} per day tamoxifen or vehicle for 4 consecutive days, then carried out analyses at different time points.

The chamber dilation in TRPV2-deficient hearts. Paraffin sections from TRPV2-deficient hearts were treated with Masson's trichrome stain and analysed histologically. After 4 days of tamoxifen treatment, hearts from $TRPV2^{flox/flox}$;$MerCreMer^{+/-}$ mice were morphologically normal with no incremental changes in the heart weight/body weight ratio or the cross-sectional area of the cardiomyocytes (Fig. 2a–d). However, 9 days after the onset of tamoxifen treatment, the chambers of the hearts from these mice were enlarged, as seen in the final phase of dilated cardiomyopathy (Fig. 2a). This dilation differed from ventricular hypertrophy as the ventricle wall was not thickened. As evidence of this, within 10 days of the onset of tamoxifen administration, the heart weight/body weight ratio and cardiomyocyte cross-sectional area in TRPV2-deficient hearts were comparable with those of control mice (Fig. 2b,c). In addition, the cardiomyocytes of TRPV2-deficient mice showed no cellular degeneration or intermuscular fibrosis (Fig. 2d). Whereas the cell–cell interfaces forming intercalated discs ran perpendicular to the muscle fibres in the hearts of $TRPV2^{flox/flox}$;$MerCreMer^{+/-}$ control mice treated only with vehicle, in hearts treated with tamoxifen for 9 days, the contact areas between cells corresponding to intercalated discs were expanded, extended and irregularly shaped (Fig. 2e). Thus, it is possible that the chamber dilation in TRPV2-deficient hearts on day 9 was associated with cellular elongation resulting from the disorganization of the intercalated disc structure. Surprisingly, about 70% of $TRPV2^{flox/flox}$;$MerCreMer^{+/-}$

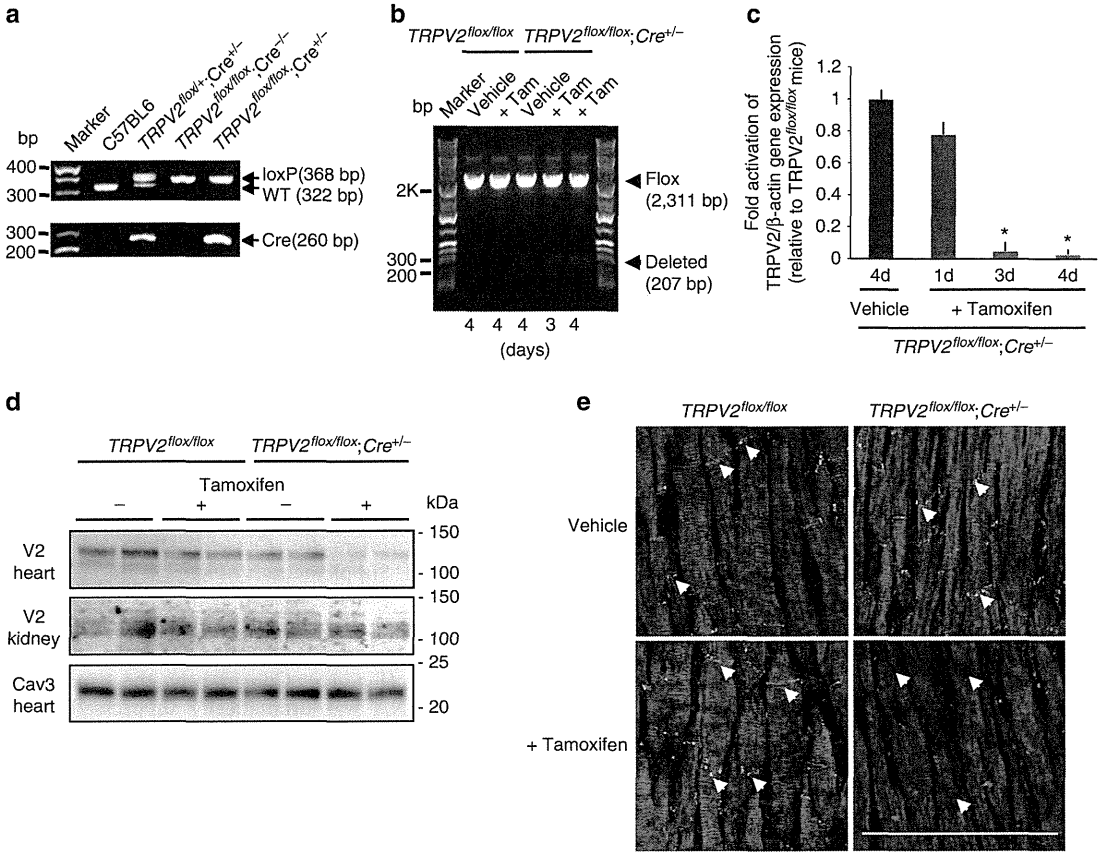

Figure 1 | Generation of temporally controlled cardiac-specific TRPV2-deficient mice. (**a**) Genotyping of *TRPV2*$^{flox/flox}$;*MerCreMer*$^{+/-}$ mice using tail genomic DNA. (**b**) Confirmation of *Cre* recombination by PCR of cardiac genomic DNA. (**c**) TRPV2 messenger RNA expression confirmed by RT-PCR, using β-actin as an internal control gene ($n=3$ mice per group). Data are mean ± s.e.m. *$P<0.05$ versus non-treated age-matched *TRPV2*$^{flox/flox}$; *MerCreMer*$^{-/-}$ (*TRPV2*$^{flox/flox}$) mice. (**d**) Expression of TRPV2 protein in heart and kidney from tamoxifen-treated and -untreated *TRPV2*$^{flox/flox}$ or *TRPV2*$^{flox/flox}$;*MerCreMer*$^{+/-}$ (*TRPV2*$^{flox/flox}$; *Cre*$^{+/-}$) mice, using caveolin 3 as an internal control for hearts. Membrane extracts (10 μg per lane) were subjected to immunoblotting. (See full blots with marker position in Supplementary Fig. 6). (**e**) Triple staining of left ventricle sections with anti-TRPV2 antibody (green), phalloidin (red) and DAPI (blue). Scale bar, 100 μm. Arrows, intercalated discs.

mice died within 10 days of the onset of tamoxifen treatment, suggesting an indispensable role for TRPV2 in the working heart (Fig. 2f).

The cardiovascular function in TRPV2-deficient mice. Echocardiography revealed a severe decline in fractional shortening and an increased left ventricular diastolic dimension 4 days after the start of tamoxifen treatment (Fig. 3a,b). Cardiac dysfunction was not observed in tamoxifen-treated *TRPV2*$^{flox/+}$; *MerCreMer*$^{+/-}$ mice (hetero knockout (KO) mice) for 4 days (Supplementary Fig. 2). Therefore, the cardiac dysfunction seen in TRPV2-deficient mice (homo KO mice) is not due to side effects associated with the overexpression of *Cre* recombinase or tamoxifen administration.

Figure 3c,d show that aortic blood pressure also gradually dropped in TRPV2-deficient mice after 3 days of tamoxifen treatment, although the heart rate did not change (Fig. 3e). Notably, the time course of blood pressure decline closely paralleled the time course of *Cre-loxP* recombination in tamoxifen-treated *TRPV2*$^{flox/flox}$;*MerCreMer*$^{+/-}$ mice (Fig. 1b,c). Therefore, the rapid reduction in blood pressure appeared to result from the severe decline in cardiac pump function following the elimination of TRPV2. This suggests that TRPV2 is critical for cardiac function under basal conditions.

The disordered intercalated discs in TRPV2-deficient hearts. Although the gross morphology of the hearts of tamoxifen-treated *TRPV2*$^{flox/flox}$;*MerCreMer*$^{+/-}$ mice after 4 days was effectively normal (Fig. 2a), the ultrastructure of the intercalated discs was already dramatically disrupted (Fig. 4a), showing extensive interdigitation, irregular shapes, lacunae and widened spaces at the sites of myofibril attachment. Immunostaining for N-cadherin and β-catenin, components of adherens junctions[4–6], showed a denser localization at cell–cell interfaces in TRPV2-deficient hearts compared with vehicle controls (Fig. 4b). The structural abnormality of intercalated disc architecture seen in *TRPV2*$^{flox/flox}$; *MerCreMer*$^{+/-}$ hearts is considered synonymous with impaired mechanical interactions with neighbouring myocytes[15]. These observations suggest that the severe decline in cardiac pump function was associated with the structural disruption of intercalated discs and adherens junctions, suggesting that mechanical coupling at these sites is under the control of TRPV2.

TRPV2 elimination affects myocardial electrical coupling. A number of cardiac disorders have been described in which disruption of the intercalated disc structure significantly affects electrical coupling[4]. In TRPV2-deficient myocytes, 4 days after the onset of tamoxifen treatment, the gap junction protein connexin 43 showed diffuse localization in the intercalated discs

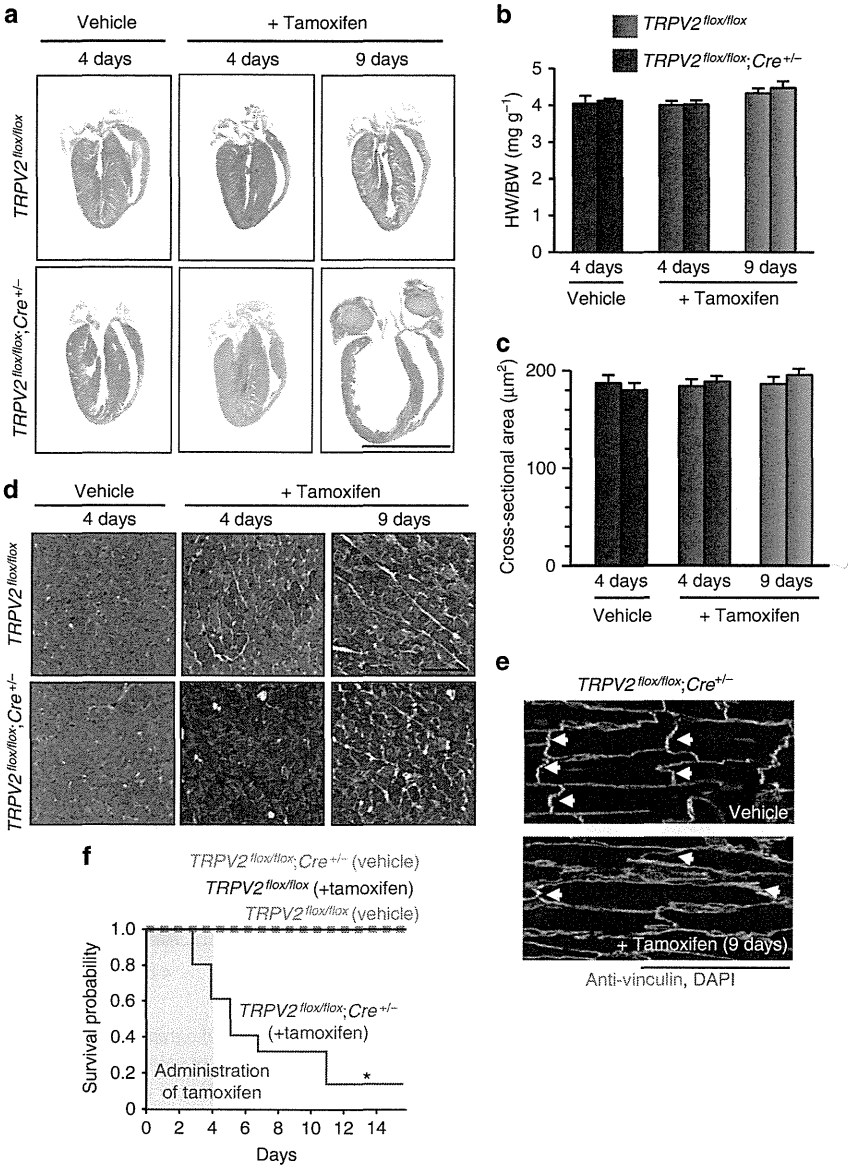

Figure 2 | Morphological changes and survival in TRPV2-deficient mice. *TRPV2*$^{flox/flox}$;*MerCreMer*$^{-/-}$ (*TRPV2*$^{flox/flox}$) and *TRPV2*$^{flox/flox}$;*MerCreMer*$^{+}$ (*TRPV2*$^{flox/flox}$;*Cre*$^{+/-}$) mice, treated with tamoxifen or vehicle, were analysed on day 4 and day 9. (**a**) Cardiac morphology. Scale bar, 5 mm. (**b**) Heart weight (HW)/body weight (BW) ratio. Data are mean ± s.e.m. (n = 22–35 hearts per group) (**c**) Cross-sectional areas from paraffin sections of left ventricles. Data are mean ± s.e.m. (n = 122–153 cells from three hearts per group) (**d**) Masson's trichrome staining of the left ventricle. Scale bar, 50 μm (**e**) Double staining with anti-vinculin antibody (green) and DAPI (blue). Scale bar, 100 μm. Arrowheads, intercalated discs. (**f**) Survival probabilities (n = 55–85 per group). *P < 0.05 versus *TRPV2*$^{flox/flox}$;*Cre*$^{+/-}$ mice treated with vehicle, by log-rank tests.

and its expression spread along the sarcolemma over time (Fig. 5a). Typical electrocardiograms obtained by telemetry showed no abnormalities over the first 4 days of tamoxifen administration (Fig. 5b); however, after 5 days, QRS complexes time-dependently widened (Supplementary Fig. 3), and 1 week after the onset of tamoxifen treatment, TRPV2-deficent hearts showed intraventricular conduction delays (Fig. 5b). As this phenomenon occurred several days after a drop in blood pressure was seen (Fig. 3c), it is likely that the disorganization of the intercalated disc architecture after the loss of TRPV2 had an indirect effect on electrical coupling with neighbouring myocytes.

TRPV2-deficient cardiomyocytes are fully functional. Abnormal Ca^{2+} handling by cardiomyocytes is a central cause of contractile dysfunction[3]. To investigate the E–C coupling of TRPV2-deficient myocytes, we analysed contractility and Ca^{2+} handling in single cardiomyocytes from tamoxifen-treated and -untreated *TRPV2*$^{flox/flox}$;*MerCreMer*$^{+/-}$ mice. Despite severe cardiac dysfunction, single myocytes isolated from these mice treated with tamoxifen for 4 days showed no abnormalities in cell morphology and shortening (Fig. 6a,b) or intracellular Ca^{2+} transients evoked by electrical stimulation (Fig. 6c), suggesting that the ablation of TRPV2 causes no significant change in intracellular Ca^{2+} handling for E–C coupling. By contrast, after 9 days of tamoxifen treatment, the isolated TRPV2-deficient cardiomyocytes showed an elongated morphology (Fig. 6a). These myocytes showed significantly impaired contractility (Fig. 6b) and Ca^{2+} cycling (Fig. 6c), compared with vehicle-treated control cells, and electrically evoked Ca^{2+} transient peaks

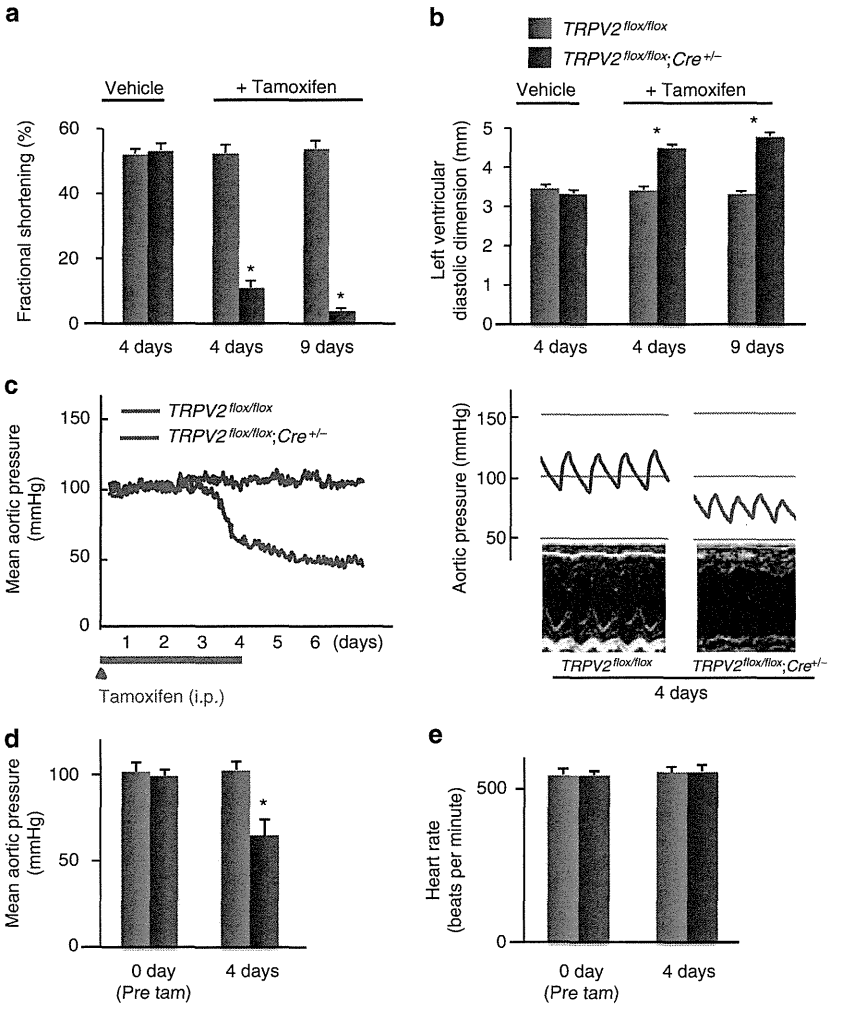

Figure 3 | Rapid, severe decline in cardiac pump function after TRPV2 elimination. (**a**,**b**) Echocardiographic parameters ($n=5$ per group). Data are means ± s.e.m. *$P<0.05$ versus $TRPV2^{flox/flox};Cre^{+/-}$ mice treated with vehicle, by two-way analysis of variance (ANOVA) with Bonferroni's *post hoc* test. (**c**) Representative pressure recording (left panel), and example of a pressure recording (upper right) and an echocardiograph (lower right) after tamoxifen treatment. (**d**,**e**) Mean aortic pressure and heart rate ($n=3$ per group). Data are means ± s.e.m. *$P<0.05$ versus all other groups, by one-way ANOVA with Bonferroni's *post hoc* test.

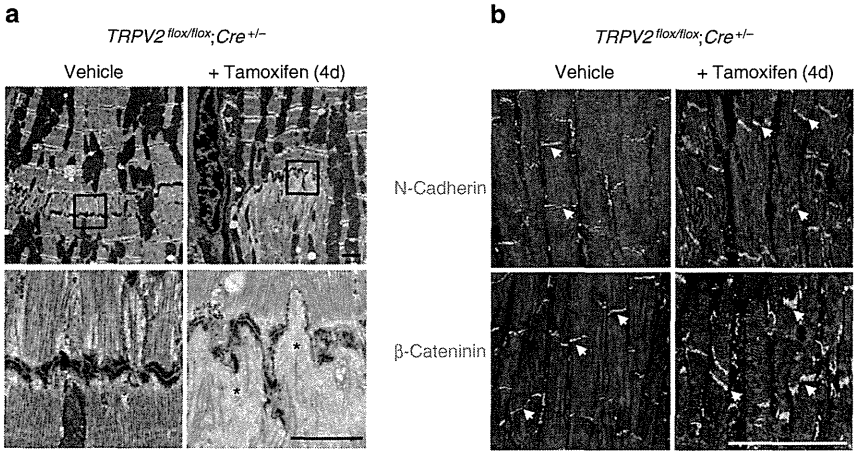

Figure 4 | Disorganization of intercalated discs in TRPV2-deficient hearts. (**a**) Electron micrographs of intercalated discs. Scale bar, 1 μm. Areas in black squares are magnified in lower panels. Asterisks, lacunae in intercalated discs. (**b**) Localization of N-cadherin and β-catenin in tamoxifen-treated $TRPV2^{flox/flox};Cre^{+/-}$ mouse hearts. Scale bar, 75 μm. Arrows, intercalated discs.